JGR Planets

RESEARCH ARTICLE
10.1029/2021JE007089

Key Points:

- Crater counting is performed to derive model ages of the layered ejecta craters (LECs) in the two candidate landing areas of Tianwen-1 mission
- The LECs likely have formed throughout the Amazonian and Hesperian periods
- The subsurface volatile concentrations in both regions might have followed different evolution lines

Supporting Information:

Supporting Information may be found in the online version of this article.

Correspondence to:

F. Zhang,
zhangfeng@nssc.ac.cn

Citation:

Niu, S., Zhang, F., Di, K., Gou, S., & Yue, Z. (2022). Layered ejecta craters in the candidate landing areas of China's first Mars mission (Tianwen-1): Implications for subsurface volatile concentrations. *Journal of Geophysical Research: Planets*, *127*, e2021JE007089. https://doi.org/10.1029/2021JE007089

Received 12 OCT 2021
Accepted 15 FEB 2022

Layered Ejecta Craters in the Candidate Landing Areas of China's First Mars Mission (Tianwen-1): Implications for Subsurface Volatile Concentrations

Shengli Niu[1], Feng Zhang[2], Kaichang Di[3,4], Sheng Gou[1,3], and Zongyu Yue[3,4]

[1]State Key Laboratory of Lunar and Planetary Sciences, Macau University of Science and Technology, Macau, China, [2]State Key Laboratory of Space Weather, National Space Science Center, Chinese Academy of Sciences, Beijing, China, [3]State Key Laboratory of Remote Sensing Science, Aerospace Information Research Institute, Chinese Academy of Sciences, Beijing, China, [4]CAS Center for Excellence in Comparative Planetology, Hefei, China

Abstract One important scientific objective of China's first Mars mission (Tianwen-1) is to investigate the martian surface soil characteristics and water-ice distribution. Layered ejecta craters (LECs) on Mars are characterized by their fluidized ejecta deposits which have been interpreted to indicate volatiles in the substrate where the impact occurred. Thus, they have potential to serve as important planetary exploration sites/targets of geological significance. In this study, we estimated the absolute model ages (AMAs) of 68 LECs with diameters >4 km using the Context Camera (an instrument onboard the Mars Reconnaissance Obiter, MRO) images in the two candidate landing areas of Tianwen-1 mission, aiming to reveal temporal-spatial variation of the regional subsurface volatiles, in particular water ice. The results from a combination of the derived AMAs and the ejecta mobility (EM) values for the southern Utopia-Isidis Planitia (SUIP) and southern Chryse Planitia (SCP) show that the LECs in both regions plausibly have formed throughout the Amazonian and Hesperian periods. However, the subsurface volatile concentrations might have undergone different evolution histories: SUIP shows a relatively stable trend with time, while there seems a general downward trend in SCP. The presence of the fresh ~1.5-km-diameter LECs suggests that volatile concentrations might have been at depth less than 150 m. We conclude with a discussion of recommendations for Tianwen-1 and future explorations that have the ability to effectively detect any signs of past and present water/ice on Mars, which contain a wealth of information of past and recent climate.

Plain Language Summary China's first mission to Mars (Tianwen-1) was launched on July 23, 2020 and successfully landed on the martian surface on 15th May 2021. Two martian surface areas were pre-selected as the potential landing sites of the mission's rover (Zhurong). To understand the regional geology in detail, we carried out an extensive investigation of a total of 68 layered ejecta craters (LECs) in both sites: the southern Utopia-Isidis Planitia and southern Chryse Planitia. A comprehensive analysis of LECs can provide key information of the structure and composition of the target substrate, subsurface volatile conditions, and their temporal variation, in particular for water ice. Using the technique of the crater size-frequency distribution measurements, these LECs are dated to have formed during the Amazonian and Hesperian epochs. The two regions might have undergone different evolution histories: subsurface volatile concentration depth of the former shows a relatively stable trend over time, while the latter appears to exhibit a general downward trend with time. The smallest observed diameters of LECs suggest that volatiles may have been at depths of hundreds of meters, even ~150 m. Both orbiter and rover radar payloads onboard Tianwen-1 would significantly help to detect potentially habitable environments in the subsurface.

1. Introduction

Distinctively different from those observed on the Moon and Mercury showing ballistic radial ejecta morphologies, martian layered ejecta craters (LECs) were first recognized in Mariner 9 imagery (McCauley, 1973) and the ejecta morphology is surrounded by distinct fluidized or lobate ejecta with relatively long runout distances in appearance, typically terminating in a distal ridge or rampart (Carr et al., 1977; Head & Roth, 1976; Mouginis-Mark, 1979). Some authors call them "rampart craters" or "fluidized ejecta craters" (Baloga et al., 2005; Mouginis-Mark, 1979, 1981; Reiss et al., 2006), but "layered ejecta crater" was suggested as a standard to better describe the morphology because it avoids reference to possible origins of these structures (Barlow et al., 2000).

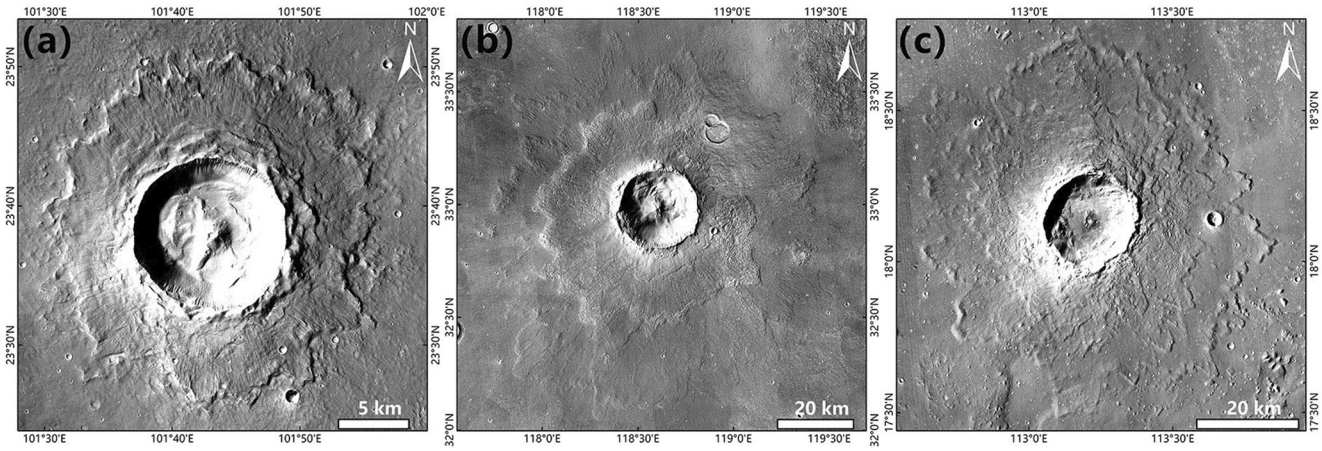

Figure 1. Three types of martian layered ejecta craters in Utopia Planitia, seen in the Mars Reconnaissance Obiter Context Camera images. (a) Single-layered ejecta crater (101.7°E, 23.6°N) displays a single blanket surrounding the crater. (b) Double-layered ejecta crater (118.6°E, 33.0°N) shows two ejecta layers, with one layer typically superimposed upon the other. (c) Multi-layered ejecta crater (113.2°E, 18.1°N) exhibits two or more ejecta layers. Typically, only the outermost layer completely surrounds the crater.

Their counterparts have not been confirmed on the Moon and other "dry", atmosphereless planets, even though some scholars have claimed the identification of impact craters with fluidized ejecta morphology on Mercury (Xiao & Komatsu, 2013). However, they have been identified on "wet", atmosphereless bodies, such as Ganymede (Boyce et al., 2010) and Charon (Robbins et al., 2018). The Mars Crater Morphology Consortium classified ejecta blankets of martian craters into three main groups: layered ejecta patterns, radial ejecta blankets, and a combination of both layered and radial patterns (Barlow et al., 2000). Based on the morphology of layered ejecta patterns, three types of LECs (Figure 1) have been proposed, including single-layered ejecta (SLE) craters, double-layered ejecta (DLE) craters, and multi-layered ejecta (MLE) craters (Barlow et al., 2000). Other sub-types of LECs, such as low-aspect-ratio layered ejecta craters (LARLE; Barlow et al., 2014; Boyce et al., 2015), excess ejecta craters (EEC; Black & Stewart, 2008), perched craters (Pr; Meresse et al., 2006), and pedestal craters (Pd; Barlow, 2006; Kadish et al., 2008, 2009), are not a focus of this study.

The formation mechanism of fluidized ejecta patterns of LECs has been debated for decades. The significant complexity and heterogeneity of their fluidized crater morphology have not been fully understood, even though abundant efforts have been made to explain the formation of LECs by involvement of surface/subsurface volatiles (e.g., water ice) which were excavated and incorporated into the ejecta during the impact process (Barlow, 2005; Barlow & Bradley, 1990; Barnouin-Jha et al., 2005; Carr et al., 1977; Kuzmin et al., 1988; Mouginis-Mark, 1979, 1981; Oberbeck, 2009; Senft & Stewart, 2008; Weiss & Head, 2013; Wohletz & Sheridan, 1983). In addition, some modeling results suggested that their formation can be ascribed to the ejecta curtain interacting with the thin martian atmosphere (Barnouin-Jha & Schultz, 1998; Schultz, 1992; Schultz & Gault, 1979). Further, a combination of atmosphere and subsurface volatiles has also been proposed and tested (Barlow, 2005; Komatsu et al., 2007; Wada & Barnouin-Jha, 2006). However, the competing roles of volatile contents in both subsurface and atmosphere in the ejecta emplacement are still debated (Komatsu et al., 2007).

Multiple lines of evidence support the subsurface volatiles scenario: (a) layered ejecta deposits were emplaced as a ground-hugging flow rather than ballistic sedimentation (Carr et al., 1977; Mouginis-Mark, 1981); (b) the onset diameters of LECs decrease with increasing latitude, consistent with the detection of depths of subsurface ice decreasing toward higher latitude (Barlow & Bradley, 1990; Costard, 1989; Kuzmin et al., 1988; Li et al., 2015; Mouginis-Mark, 1979; Squyres et al., 1992); (c) a few laboratory studies and numerical simulations of impact into water or ice-rich targets suggest that the near-surface icy layer might have triggered layered ejecta morphologies on Mars (Baloga et al., 2005; Senft & Stewart, 2008); and (d) craters with layered ejecta morphologies on the Ganymede (Boyce et al., 2010) and Charon (Robbins et al., 2018) without atmosphere further indicates that the atmosphere action is not a necessary condition for layered ejecta morphology formation, and the subsurface volatiles may be the dominant formation mechanism of the LECs on Mars.

Under the assumption that the formation mechanism of LECs is related to subsurface ice deposits (e.g., a volatile-rich target), LECs are potential probes of subsurface volatile conditions (e.g., Weiss & Head, 2014). The emplacement of their ejecta has been interpreted to be sensitive to subsurface stratigraphic conditions, such as volatile content, particle size, layer thickness and cohesion (Jones et al., 2016). Therefore, more-than-one layer ejecta craters are typically interpreted as resulting from an impact into a multi-layered target with a gradient in particle size distribution and/or volatile content (Boyce & Mouginis-Mark, 2006; Senft & Stewart, 2008; Weiss & Head, 2013).

In order to quantitatively characterize the mobility and viscosity of the subsurface materials excavated, a parameter named ejecta mobility (EM) has been defined as the maximum radius (runout distance) of the continuous ejecta deposits or the deposits' average extent measured from the crater rim to crater radius (Barlow, 2004; Costard, 1989; Weiss & Head, 2014). It is normalized by the parent crater's radius to eliminate the effect of different crater sizes (Mouginis-Mark, 1979). EM has thus been considered as a useful indicator for quantitatively measuring the degree of ejecta fluidity, which likely provides information to qualitatively constrain the conditions (e.g., volatile concentrations) under which the impact occurred (Barlow, 2004; Weiss & Head, 2014). In addition, the minimum diameter of regional LECs is limited by the local near-surface water ice conditions and called onset diameter (Barlow et al., 2001; Barlow & Perez, 2003; Kuzmin, 1980). The onset diameter, therefore, can be used to estimate the depth of the subsurface ice (e.g., Kuzmin et al., 1988).

Using a combination of EM and onset diameter of LECs, many previous efforts have been made to map regional or global ground ice distribution on Mars (Barlow & Bradley, 1990; Costard, 1989; Kuzmin et al., 1988; Mouginis-Mark, 1979; Squyres et al., 1992). The mapping results revealed that EM values vary among different ejecta types and locations, suggesting that volatile concentrations vary with locality (Barlow, 2004; Costard, 1989; Mouginis-Mark, 1979, 1981). This relevance of EM variations with location is supported by the proposed distributions of subsurface volatiles from theoretically modeling results (Clifford, 1993; Fanale et al., 1986) and the observed global distribution of near-surface water-equivalent hydrogen concentrations detected by the Gamma-Ray Spectrometer instrument suite (Boynton et al., 2002; Feldman et al., 2004) and the Thermal Emission Imaging System (Bandfield, 2007) onboard Mars Odyssey spacecraft (Saunders et al., 2004).

Squyres et al. (1992) pointed out that LECs may have formed during an unusual geological epoch and the onset diameter reflects the depth of subsurface volatiles at a given time. However, the spatial distribution and temporal evolution of subsurface ice at the regional level remain only sparsely investigated in detail (Barlow, 2004; Kirchoff & Grimm, 2018; Lagain et al., 2021; Noe Dobrea et al., 2020; Reiss et al., 2006; Viola et al., 2015). Barlow (2004) compared preservation class (a proxy for time) with its EM of LECs to determine whether subsurface volatiles concentrations have changed over time. The regional analysis results indicated that subsurface volatiles concentration remained almost constant over time. In contrast, using the technique of the crater size-frequency distribution (CSFD) measurements, Reiss et al. (2006) derived the absolute model ages (AMAs) of LECs in three equatorial regions revealing a volatile-rich period in the Early Hesperian and generally, an increasing-depth trend of the ground ice table with time afterward. Kirchoff and Grimm (2018) have carefully dated 10 Amazonian-aged (<3 Ga) and 10 Hesperian-aged (between 3.0 Ga and 3.7 Ga) SLE craters in the tropics by measuring small craters superposed on their continuous ejecta blankets. Their results suggest that there was still underground ice at a depth of several hundred meters in the youngest Amazonian epoch on Mars. Subsurface ice has even detected with recent missions at a few cm to tens of meters deep at high latitudes (Mellon et al., 2009; Noe Dobrea et al., 2020).

In this work, under the assumption that LECs are related to subsurface volatiles, we presented a detailed investigation of multiple parameters (i.e., AMAs, EM, and onset diameter) associated with the LECs in the two candidate landing areas (see Section 2) of China's first Mars exploration mission (Tianwen-1; Ye et al., 2017; Wan et al., 2020). Determining the AMAs of LECs, understanding the mode of emplacement of layered ejecta, their morphology, morphological characteristics (e.g., EM), and the role of volatiles that might have played in their formation are critical to estimating the regional volatile history and to developing our knowledge of these features. We focus on the two candidate landing areas for the following three main reasons. First, a series of landforms are found to be related to water or ice in these areas, such as LECs, outflow channels, deltas, thumbprint terrain, wrinkle ridges, thermokarst, polygonally fractured ground, and ice-cored mounds. Second, the two areas are located on the north-south hemisphere dichotomy boundary of Mars, containing clues to structural and compositional evolution of both distinct terrains due to a complex history of water activity (Carr & Head, 2010).

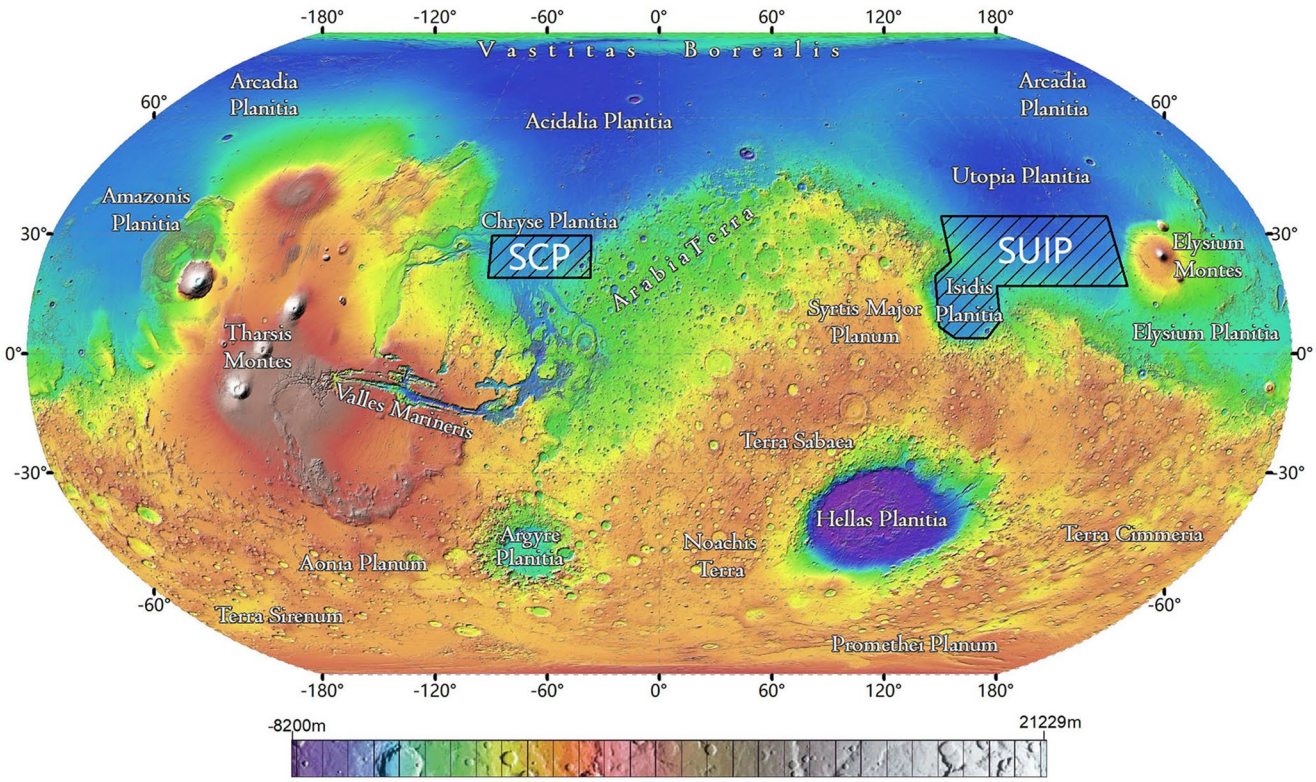

Figure 2. The regional context of the study areas (black boxes): the southern Utopia-Isidis Planitia (SUIP) and southern Chryse Planitia region (SCP). SUIP includes the southern Upotia Planitia (85–134°E and 17–34°N) and the whole Isidis Planitia (80–98°E and 4–20°N), and SCP includes the southern Chryse Planitia (20–50°W and 20–30°N). Basemap is the Mars Orbiter Laser Altimeter shaded relief map (The Robinson map projection is used).

Finally, this would provide deep insights into the groundwater ice conditions assisting in identifying potential scientific survey targets for China's first and other future Mars exploration missions.

2. Tianwen-1 Mission and Geological Settings of the Study Regions

2.1. Tianwen-1 Mission

China's first Mars exploration mission (Tianwen-1) was launched from the Wenchang Spacecraft Launch Site on July 23, 2020, and successfully landed on May 15, 2021. It is composed of an orbiter, a lander, and a rover. Given the rover's requirement for touchdown safety and mobility, two candidate landing areas were selected for the Mars exploration mission in the latitude range of 5–30°N (Ye et al., 2017; B. Wu, Dong, et al., 2021): the southern Utopia-Isidis Planitia (SUIP) and southern Chryse Planitia (SCP; Figure 2). Although the Tianwen-1 mission landed in Utopia Planitia at 109.925°E, 25.066°N (e.g., Liu et al., 2021; Mills et al., 2021; Wan et al., 2021; X. Wu, Liu, et al., 2021; Zhao et al., 2021), our analysis included both candidate areas as mentioned above for full documentation and comparison purposes. In general, the scientific objectives of the mission are to conduct field geological mapping, investigate the surface soil characteristics and material composition, detect water-ice distribution, and explore the atmospheric ionosphere and surface climate and environment conditions. Further, a study of the history of early geological evolution and internal mass distribution will be performed by characterizing the martian electromagnetic and gravitational field (Wan et al., 2020).

2.2. Southern Utopia-Isidis Planitia

The SUIP (Figure 2) contains the southern Utopia Planitia (85–134°E and 17–34°N) and the whole Isidis Planitia (80–98°E and 4–20°N). It is surrounded by Elysium Montes to the east, the Syrtis Major Planum to the southwest, the Libya Montes and the Nepenthes Mensae to the south, and the center of the Utopia Planitia to the north (Figure 2).

An extensive reservoir of water in the southern Utopia Planitia is inferred from several terrain types. These geologic features include: (a) heavily degraded/buried craters (McGill, 1986) occurring throughout Utopia Planitia. Their morphology and topography were interpreted as evidence of compaction of possibly sedimentary materials of the Vastitas Borealis against the rims of buried craters (Buczkowski & McGill, 2002); (b) thumbprint terrains (TPT) located on the southern edge of Utopia Planitia (Lockwood et al., 1992). A variety of hypotheses has been proposed for their formation, such as glacial (Grizzaffi & Schultz, 1989) and volcanic (Ghent et al., 2012) origin. Whatever the case, the presence of a large amount of ice/water is a requirement; (c) giant polygonal patterned grounds occurring peripheral to the center of the Utopia basin (McGill, 1986). The presence of a large standing body of water/ice or subsurface water has been suggested to the critical elements of the formation of these terrains (Hiesinger & Head, 2000); (d) impact craters with layered ejecta and pancake-like ejecta (Mouginis-Mark, 1979); (e) numerous putative periglacial landforms comprising relatively shallow, flat-floored and scalloped depressions, small-sized polygons, and polygon trough/junction pits (e.g., Séjourné et al., 2011; Soare et al., 2012); and (f) wide distribution of water-related pitted cones that have been attributed to mud volcanism (McGowan, 2011 and references therein).

Isidis Planitia (centered at 14°N, 88°E) is located inside a multi-ring impact crater with a diameter of approximately 1,200 km in the eastern hemisphere of Mars along the crustal dichotomy (Wichman & Schultz, 1989). Several terrain types are found in Isidis Planitia, including an annulus of ridged terrain, knobby terrain, hillocky terrain (Grizzaffi & Schultz, 1989), and TPT (Lockwood et al., 1992). Ivanov et al. (2012) divided the geologic history of Isidis Planitia into three principal episodes: (a) impact dominated episode (Noachian, until ~3.8 Ga), followed by resurfacing of later volcanism and fluvial/glacial activity; (b) more volcanism and fluvial/glacial processes dominated episode (late Noachian-early Amazonian, ~3.8–2.8 Ga), with fluvial/glacial activity leading to a major resurfacing of Isidis Planitia during the later phase (mostly at ~3.4–3.1 Ga); and (c) aeolian-dominated episode (since early Amazonian, ~2.8 Ga). The southern rim of the Isidis basin was preserved as a series of dissected massifs (i.e., the Libya Montes), which represent remnants of ancient Noachian highlands and appear heavily modified by fluvial activity and contains a high density of valley networks on Mars (Crumpler & Tanaka, 2003). The morphology of the Deuteronilus paleoshoreline in the south edge of the Isidis basin suggests that there was once a frozen sea in the Late Hesperian/Early Amazonian period, and as the ice melted and sublimated it left traces of past subglacial erosion and deposition on the surface of Isidis Planitia (Erkeling et al., 2012, 2014; Guidat et al., 2015).

The new geologic map of Mars updated and compiled by Tanaka et al. (2014) shows that most of SUIP is covered by the late Hesperian lowland unit (lHl) which in both basins is separated by the late Hesperian transition unit (lHt; Figure 3a). The hundreds of meters to kilometers thick lHl deposits are interpreted as fluvial/lacustrine/marine and colluvial sediments sourced from circum-lowland outflow channels and adjacent highland terrains, likely underlain by igneous rocks and modified and covered by later water- and wind-related surface processes and products (Tanaka et al., 2014). The unit lHt occurs along highland/lowland boundary and mainly comprises plains-forming deposits with relatively smooth surfaces, which are considered of multiple origins, including mass-wasting, fluvial/lacustrine, and possibly other sedimentary materials and volcanic rocks in places (Tanaka et al., 2014). The Amazonian Hesperian volcanic unit (AHv) is mainly composed of lava flows accumulated around Elysium Montes. Other geologic units labeled in Figure 3a are less focused in this study, the detailed information can be found in the work of Tanaka et al. (2014).

2.3. Southern Chryse Planitia

The Chryse Planitia (20–50°W and 20–30°N) is a highland-lowland boundary plain just north of the martian equator near the Tharsis region to the west (Figure 2). It is not a locally closed depression or basin but instead opens into the northern lowlands. The SCP is the focal point of the end of many outflow channels (i.e., Kasei, Maja, Simud, Tiu, Ares, and Mawrth Valles) from the southern highlands as well as from Valles Marineris and the flanks of the Tharsis bulge (Carr, 1996). Various hypotheses have been proposed to interpret the origin of these channels, including catastrophic flood processes (Golombek et al., 1997), liquefaction mudflows (Nummedal & Prior, 1981), glacial processes (Lucchitta, 1982), and mass or debris flows (Tanaka, 1999). The analysis of channel morphologies supports the requirement of a significant volume of water flowing into a shallow submarine environment (e.g., Di Achille & Hynek, 2010; Ivanov & Head, 2001; Parker et al., 1989), consistent with the hypothesis of possibly large ocean-scale standing bodies of water occupying the northern lowlands

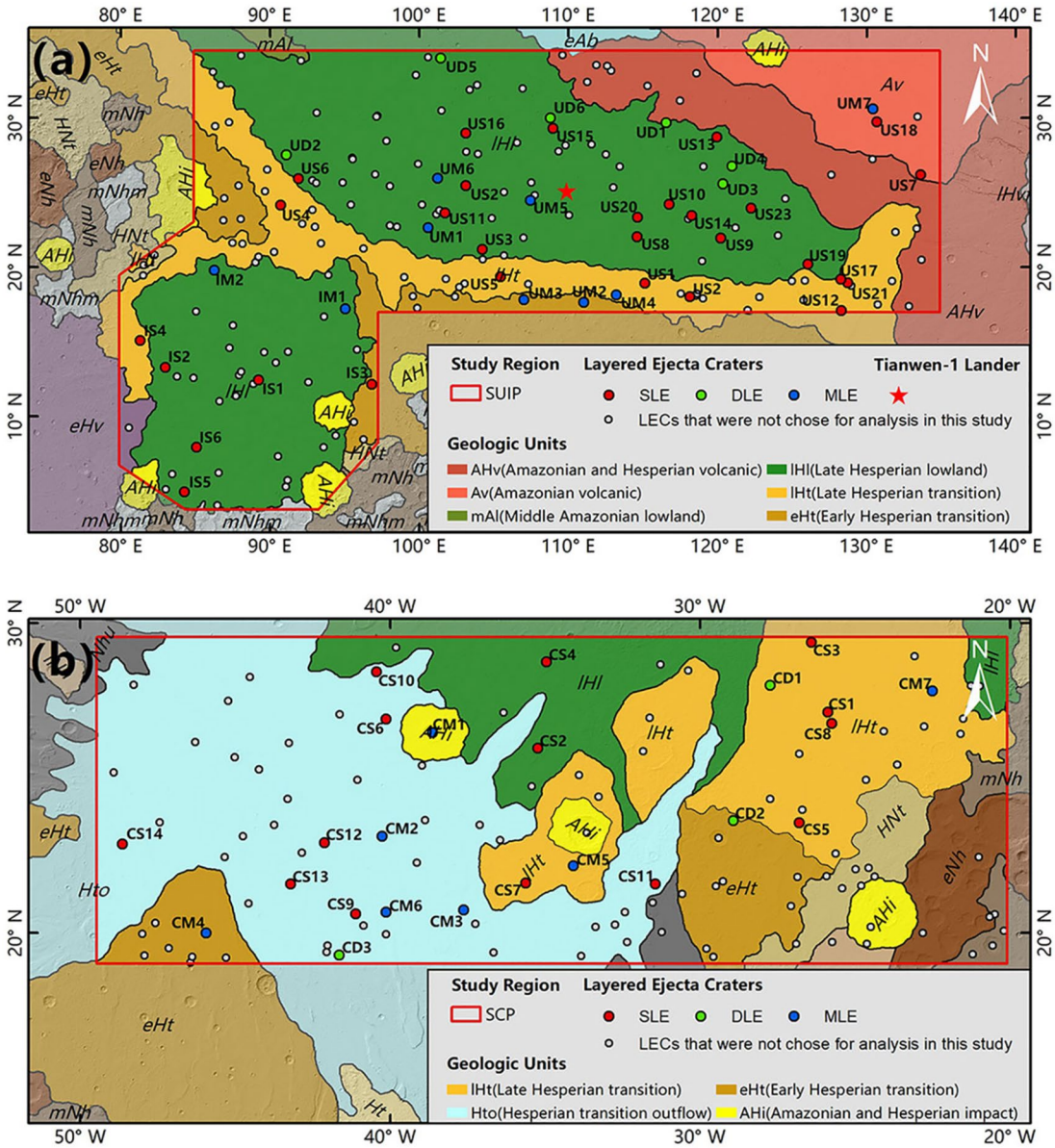

Figure 3. Geological maps of the two study regions: southern Utopia-Isidis Planitia (SUIP) and southern Chryse Planitia region (SCP; red polygons), constructed from shapefiles (Tanaka et al., 2014) overlain on a Mars Orbiter Laser Altimeter shaded relief map. (a) The distribution map of layered ejecta craters (LECs) in SUIP region. Among them, a total of 44 LECs are identified as study targets. The red star near to the LEC UM5 illustrates the landing site of Tianwen-1 lander. (b) The distribution map of LECs in SCP region. Of these, 24 LECs are chosen for analysis in this study. The red, green and blue points respectively indicate the single-layered ejecta (SLE), direct-layered ejecta (DLE) and multi-layered ejecta (MLE) craters. Gray points without labels mark the locations of other LECs that were not analyzed in this study. The nomenclature of the studied LECs is defined as a combination of the initials of their host basin name (i.e., U-Utopia Planitia, I-Isidis Planitia, and C-Chryse Planitia), first letter of LEC type (i.e., S-SLE, D-DLE, M-MLE), and a number. Numbers are arranged in descending order of age.

in Hesperian-Early Amazonian times (Head et al., 1999). The circum-Chryse outflow channels were estimated to have mainly formed in the Hesperian (Head et al., 2002; Ivanov & Head, 2001), but become younger as the distance to the Chryse basin decreases (Moore et al., 1995). Several landforms are found in the SCP, including wrinkle ridges, knobs and mounds, and teardrop-shaped islands (Greeley et al., 1977). The distribution of many small LECs within the basin was proposed to indicate subsurface shallow volatile concentrations (Demura & Kurita, 1998). The SCP is largely dominated by the Hesperian transition outflow (Hto) unit, which is mainly composed of outflow channel sediments and carved by the channel systems (Tanaka et al., 2014). The rest is mainly covered by the lHt unit and early Hesperian transition (eHt) unit (Figure 3). Relative to lHt, the unit eHt

is interpreted as undulating to moderately rugged plain-forming deposits, mainly composed of mass-wasting, fluvial/lacustrine, and other sedimentary materials from nearby highland outcrops (Tanaka et al., 2014).

3. Data and Methods

3.1. Data Sets Used in This Study

In this work, we used two categories of data sets: imagery acquired by a variety of missions and the recently updated geologic map of Mars constructed by Tanaka et al. (2014). Image data sets include images acquired by the Context Camera (CTX) onboard the Mars Reconnaissance Orbiter (Malin et al., 2007) and Thermal Emission Imaging System (THEMIS) on Mars Odyssey (Christensen et al., 2004). The CTX images (~6.0 m/pix) have nearly covered the entire Mars surface. The Bruce Murray Laboratory for Planetary Visualization has produced a mapped, semi-controlled mosaic of Mars rendered at 5.0 m/pixel using CTX images. The CTX mosaic has achieved near-global (97.3%) coverage of Mars. This database are divided into $4° \times 4°$ and $2° \times 2°$ tiles, which are publicly available online (http://murray-lab.caltech.edu/CTX/tiles/). A total of 122 CTX mosaic tiles ($4° \times 4°$) is used in SUIP (90 CTX mosaic tiles) and SCP (32 CTX mosaic tiles) regions. Single CTX images used in this study to fill the gaps of the CTX mosaic are archived in the Planetary Data Systems (PDS) Geosciences Node (https://ode.rsl.wustl.edu/mars/) or Mars Image Explorer website (http://themis-data.asu.edu/viewer/ctx#T=0). The THEMIS data includes multi-spectral thermal-infrared (IR) images (100 m/pix) and visible/near-IR images (18 m/pix). Edwards et al. (2011) produced the seamless global image mosaic (100 m/pix) using THEMIS daytime IR images. This mosaic is also available online (https://astrogeology.usgs.gov/search/map/Mars/Odyssey/THEMIS-IR-Mosaic-ASU/Mars_MO_THEMIS-IR-Day_mosaic_global_100m_v12). The CTX mosaic tiles and individual images and the THEMIS daytime IR seamless global mosaic are used to identify LECs and small craters located within their ejecta deposits. These small craters are used to perform crater count dating of LECs. The morphologic parameters (e.g., crater diameter, ejecta dimensions) of LECs are also measured using the imagery mentioned above. Additionally, the updated geologic map of Mars (Tanaka et al., 2014) is used to analyze the geologic settings of the study regions, which is available via the following URL: https://pubs.usgs.gov/sim/3292/.

A total of 286 LECs in both study regions (SUIP:175, Figure 3a; SCP:111, Figure 3b) have been collected by Li et al. (2015) and Robbins and Hynek. (2012). Of them, a subset of 68 LECs with diameters of >4 km are selected for analysis based on the following three factors considered. First, the ejecta blankets should have enough area so that superposed craters can be measured. Second, the ejecta blankets are complete and well-preserved, thus minimizing the degrees of influence by subsequent surface processes. And third, the selected LECs are relatively uniformly distributed in the study areas, indicating that these LECs are representative of regional phenomenon rather than just local. Thus, a total of 44 and 24 LECs in SUIP and SCP were selected (red, green, and blue points in Figures 3a and 3b), respectively. Existing LEC databases (e.g., Li et al., 2015; Robbins & Hynek, 2012) were constructed based on the martian ejecta morphology using THEMIS daytime images (100 m/pixel) following the classification criteria from Barlow et al. (2000). Nevertheless, it is worthwhile to update the classification scheme with current high-resolution image data (e.g., 5 m/pixel CTX image, Weiss & Head, 2014) and more specific classification criteria summarized by Barlow (2015). Though we did not re-evaluate all the LECs in both study regions, the selected 68 LECs in this study were confidently classified by a combination of our careful observations and the classification criteria widely adopted in many previous studies (e.g., Barlow, 2015; Barlow et al., 2000; Li et al., 2015; Robbins & Hynek, 2012; Weiss & Head, 2014). The detailed information of these LECs (i.e., location, ejecta morphology and geologic units) can be found in the Supporting Information (Tables S1 and S2).

3.2. Methods

We have evaluated each LEC in ArcGIS using the CTX image mosaics (5.0 m/pix) and THEMIS daytime IR global mosaic (100 m/pix). First, for each LEC the counting area for superposed craters were manually defined as the closed area between the distal border of the continuous ejecta blankets and the inner border, which is defined as a 20% crater radius away from the crater rim crest (e.g., Lagain et al., 2021; Robbins & Hynek, 2012; Figure 4a). This results in more accurate AMAs by minimizing the effect of resurfacing processes that might have occurred at the rim zones due to its inherent topography (sliding slope, aeolian erosion…). The diameter of the

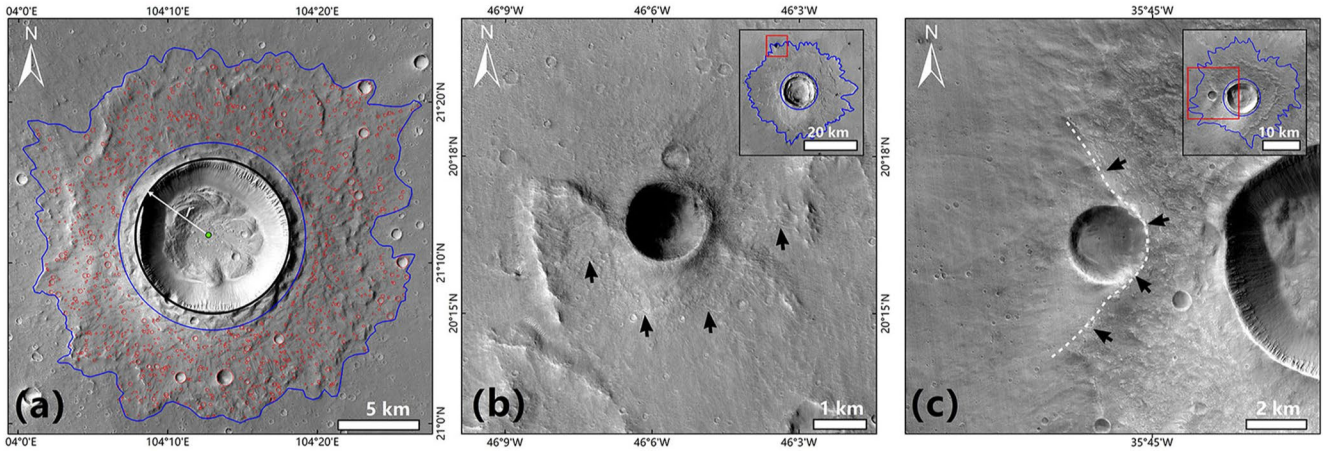

Figure 4. Layered ejecta craters (LEC) examples showing how we delineate the outline of ejecta deposits and identify superposed craters. (a) The area enclosed by the blue lines indicates the crater count area, and the black solid line illustrates the 3-point circle crater rim measurement. The green point marks the center of the crater. The red circles represent manually identified superposed craters on the continuous ejecta blankets. (b) A post-LEC crater exhibits radial and concentric ejecta traces (black arrows) on the surface of the ejecta of the host LEC. The inset image in the upper right corner shows the location (the red box) of the relationship. (c) A pre-LEC crater shows that its east rim and ejecta deposits are buried, covered, and bypassed by fluidized ejecta of the LEC. The red box in the inset image in the upper right corner indicates the location of the relationship. The white dashed line and the black arrows mark the distal boundary of the ejecta blanket of the LEC.

crater is calculated through fitting a circle to three points mapped on the crater rim. This process is performed with the assistance of ArcGIS add-in "Crater Tools" (Kneissl et al., 2011). Then, the basic characteristic parameters (i.e., crater diameter, crater area, and ejecta area) of LECs are calculated automatically and stored as a shapefile in ArcGIS. This provides the basis for the following CSFD dating (see Section 3.2.1), calculation of EM values (see Section 3.2.2), and estimating crater excavation depth (see Section 3.2.3).

3.2.1. Superposed Crater Identification and Dating

To estimate the AMAs of these LECs, we counted and measured small craters confined within the outline of their ejecta blankets (Figure 4a). All craters counting measurements were carried out in ArcGIS add-in "Crater Tools," which automatically adjust the map projection to avoid measurement errors (Kneissl et al., 2011). To improve the quality of AMAs, we excluded secondary craters as much as possible, which often show a concentration in clusters and/or chains, irregular and shallow shapes, and distinctive herring-bone patterns. In addition, we carefully examined craters by checking their stratigraphic relationship with the substrate to ensure that these craters were formed after the ejecta deposits. For example, craters postdating the host LEC commonly display clear and/or subtle radial and/or concentric ejecta traces preserved on the surface of the LEC's ejecta blanket (Figure 4b). As a contrast, pre-existing craters and their surrounding ejecta deposits would be partially buried, covered, and bypassed by fluidized ejecta of the LEC that was formed after the crater (Figure 4c). Because the crater identification is subject to image resolution, we only identified craters with diameters greater than 50 m in CTX images. All the above operations were completed in ArcGIS, and then CSFD data was generated.

We analyzed the CSFD data using the Craterstats software (Michael, 2013; Michael & Neukum, 2010). To derive AMAs and associated uncertainties of LECs, we used the chronology function (CF) of Hartmann and Neukum (2001) and the production function (PF) of Ivanov (2001) by Poisson timing analysis technique (Michael et al., 2016), along with epoch boundaries refined by Michael. (2013), and randomness analyses by the mean second-closest neighbor distance (M2CND; Michael et al., 2012). The Poisson timing analysis technique was used because it does not need to consider the choice of binning width, the application of any type of curve fitting technique and the number of craters in the statistical area (Michael et al., 2016).

The nomenclature of the studied LECs in both regions (Figures 3a and 3b) is defined as a combination of the initials of their host basin's name (i.e., U-Utopia Planitia, I-Isidis Planitia, and C-Chryse Planitia), first letter of LEC type (i.e., S-SLE, D-DLE, M-MLE), and a number. Numbers are arranged in descending order of age: the smaller the number, the older the LEC. Based on these rules, the LEC named CS1 represents a SLE crater located in Chryse Planitia, and the number 1 indicates that it is the oldest SLE crater examined.

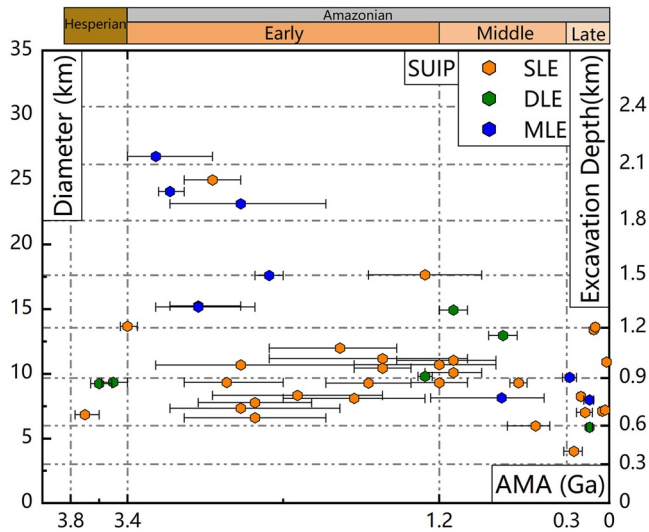

Figure 5. Scatter plot of diameters versus absolute model ages and derived excavation depths of the 44 layered ejecta craters (LECs) in southern Utopia-Isidis Planitia. The numbers of single layered ejecta (yellow), double layered ejecta (green), and multi layered ejecta (blue) craters are 29, 6, and 9, respectively. The majority of all the LECs have diameters between 5 and 20 km. Model age bins are based upon the epochs of Michael (2013) using the Neukum chronology: <0.3 Ga (Late Amazonian), 0.3–1.2 Ga (Middle Amazonian), 1.2–3.4 Ga (Early Amazonian), 3.4–3.8 Ga (Hesperian), and >3.8 Ga (Noachian).

3.2.2. Evaluation of Ejecta Mobility (EM) of LECs

The EM value of individual LECs is defined as the runout distance of continuous ejecta blankets from the crater rim normalized by the crater radius (Barlow, 2004, 2005; Costard, 1989; Mouginis-Mark, 1979). Generally, runout distance and its derived EM value have two different definitions (Robbins & Hynek, 2012). One uses the average ejecta extent as the "runout distance", which is suggested to provide a characterization of the overall energy and viscosities involved (e.g., Barlow, 2005, 2006). The other uses the maximum extent of the ejecta deposits to indicate the "runout distance", which plausibly represents the largest distance the cohesive ejecta could reach given the impact energy available (e.g., Costard, 1989; Mouginis-Mark, 1979). However, the EM values may be influenced by many factors (e.g., the viscosity of the ejecta flow, slope/roughness of the pre-existing surface and the size distribution of clasts within the ejecta, etc), and in particular the runout distance of the ejecta is the most vulnerable to slope/roughness of the pre-existing surface, which would cause non-uniform diffusion of the ejecta to the surroundings. Thus, we used the first definition to calculate EM values. Doing so weakens other effects as much as possible and highlight the effect of volatile concentration. The formula is listed as follows:

$$EM(Ejecta\ \ Mobility) = \frac{\sqrt{A_{ejecta+crater}/\pi} - r_{crater}}{r_{crater}}$$

where $A_{ejecta+crater}$ is a total enclosed area inside the outline of layered ejecta deposits (i.e., the sum of the ejecta area and the crater area), the r_{crater} is the radius of the LEC (Figure 4a).

3.2.3. Estimating Crater Excavation Depth

The LEC diameter can estimate the depth of excavation locally, which may provide the depth information of subsurface ice (Barlow et al., 2001; Kuzmin et al., 1988). To estimate an approximate lower limit of the depth of the possible subsurface ice table (very local just around the crater), we derived the excavation depth (d_e) of the LECs as $d_e = 0.1D_t$ based on the relationship developed by Melosh (1989), where D_t is the transient diameter of the crater. For large craters ($D_r > 6\ km$), where $D_t = D_{sc}^{0.15\pm0.04} D_r^{0.85\pm0.04}$ (Croft, 1985), the D_r is the crater rim-to-rim diameter, and the D_{sc} is the simple to complex transition diameter, which is usually ~6 km for Martian craters (Robbins & Hynek, 2012). For small craters ($D_r \leq 6\ \ km$), the simple relationship $D_t = D_r$ (Barlow, 2005) is adopted.

4. Results

The details of 68 LECs selected that met our requirements (see Section 3.1), particularly that the ejecta blankets were not considerably modified, are summarized in the Supporting Information (Tables S1 and S2). Table S1 reports the AMAs, EM, and excavation depth of 44 LECs in SUIP. Table S2 reports the AMAs, EM, and excavation depth of 24 LECs in SCP. We now turn to a detailed description of these results below.

4.1. Distribution of LECs

The distributions of ejecta morphologic types of the studied LECs in both SUIP and SCP (Figures 3a and 3b) show a similar trend. The number of SLE craters in SUIP occupies more than half of the total number of all studied LECs (SLE: DLE: MLE = 29:6:9), as well as the case for the types of LECs in SCP (14:3:7). The majority of all the LECs in both SUIP and SCP have diameters between 5 and 20 km (Figures 5 and 6). Note, only one LEC (SLE) crater smaller than 5 km is identified, with none in the SCP. The largest LEC in SUIP is ~27 km in diameter, and ~33 km in SCP (Figures 5 and 6; also see the detail in the Supporting Information: Tables S1 and S2). The largest LECs in both SUIP and SCP are MLE craters.

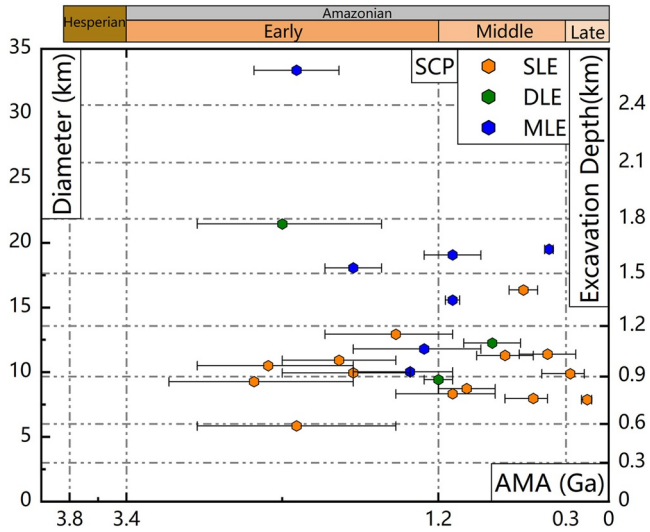

Figure 6. Scatter plot of diameters versus absolute model ages and derived excavation depths of the 24 layered ejecta craters (LECs) in southern Chryse Planitia. The numbers of single layered ejecta (yellow), double layered ejecta (green), and multi layered ejecta (blue) craters are respective 14, 3, and 7. The majority of all the LECs have diameters between 5 and 20 km. Model age bins are based upon the epochs of Michael (2013) using the Neukum chronology: <0.3 Ga (Late Amazonian), 0.3–1.2 Ga (Middle Amazonian), 1.2–3.4 Ga (Early Amazonian), 3.4–3.8 Ga (Hesperian), and >3.8 Ga (Noachian).

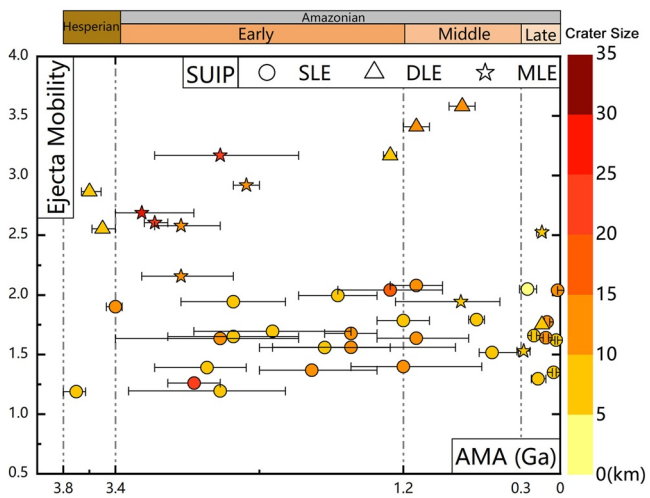

Figure 7. Scatter plot of the ejecta mobility (EM) values versus absolute model age of the 44 layered ejecta craters (LECs) in southern Utopia-Isidis Planitia region. The color variation from light yellow to deep red indicate LEC diameters with an increasing trend. The 29 single layered ejecta (SLE craters (circles) have a narrow EM value range between 1.0 and 2.0 with no trend with time. The direct layered ejecta craters (triangles) exhibit EM values (most >2.5) significantly larger than that of the SLE craters (all <2.0). The multi layered ejecta craters (stars) younger than 1.2 Ga have relatively lower EM values (2.5 or smaller) than that (most >2.5) of those older than 2.0 Ga.

4.2. Absolute Model Ages

4.2.1. AMAs of LECs in SUIP Region

The dating results of 44 LECs in SUIP region show AMAs ranging from $\mu 22^{+6}_{-5}$ Ma to $\mu 3.7^{+0.07}_{-0.1}$Ga (Figure 5). Among them, 36 LECs are in southern Utopia Planitia ($\mu 22^{+6}_{-5}$Ma to $\mu 3.7^{+0.07}_{-0.1}$ Ga), and eight in Isidis Planitia ($\mu 1.1^{+0.4}_{-0.3}$ to $\mu 2.9^{+0.3}_{-0.4}$ Ga; Figure 3a). Based on the epoch scheme by Michael (2013), 11 LECs were formed in the late Amazonian (<0.3 Ga), nine in the middle Amazonian (0.3–1.2 Ga), 21 in the early Amazonian (1.2–3.4 Ga), and only three in the Hesperian (3.4–3.8 Ga; Figure 5).

4.2.2. AMAs of LECs in SCP Region

The derived AMAs of 24 LEC samples in SCP range from $\mu 0.15^{+0.04}_{-0.03}$ Ga to $\mu 2.5^{+0.6}_{-0.7}$ Ga (Figure 6). All LECs samples were formed during the Amazonian period: only two LEC was formed in the late Amazonian (<0.3 Ga), 11 in the middle Amazonian (0.3–1.2 Ga), 11 in the early Amazonian (1.2–3.4 Ga), and no LECs were found in the Hesperian (3.4–3.8 Ga; Figure 6).

Importantly, it should be noted that the AMAs of all the LECs in both SUIP and SCP areas are not indicated as a function of crater size, which can be seen from Figures 7 and 8. In both figures, different symbols (circles, triangles, and stars) denote the three different LEC types (i.e., SLE, DLE, and MLE), and diameters of LECs are indicated by color with size increasing from light yellow to deep red.

4.3. Ejecta Mobility of LECs

4.3.1. Ejecta Mobility in SUIP Region

Some regular trends of the three morphologic types of LECs (i.e., SLE, DLE and MLE) in SUIP can be observed from our derived results. The EM values of all the 29 SLE craters are concentrated between 1.0 and 2.0 (i.e., around 1.5), and show no regular change with time (Figure 7). Nearly all the DLE craters have EM values larger than 2.5 but except for the youngest one showing a lower EM value ~1.8. In comparison, however, the EM values of the nine MLE craters display a general decreasing trend over time. For the six older MLE craters (AMAs between 2.3 and 3.4 Ga in Early Amazonian), they commonly have EM values larger than 2.5 but only one ~2.2 (Figure 7). As a contrast, the three younger MLE craters (AMAs between 0 and 1.2 Ga in Middle to Late Amazonian) show EM values between 1.5 and 2.0 with the youngest one ~2.5 (Figure 7). Furthermore, Figure 7 indicates that EM values are not a function of crater size: some smaller LECs have higher EM values, while some larger ones exhibit lower EM values.

4.3.2. Ejecta Mobility in SCP Region

As s striking contrast, all LECs (SLE, DLE, and MLE) in SCP exhibit a generally decreasing trend in average EM values with time. As a whole, all the LECs display EM values ranging from larger than 2.5 to ~1.0. Most LECs have EM values lower than 2.5, with only three slightly larger than 2.5 (Figure 8). Generally, the MLE craters show no regular EM value trend with time, while the three DLE craters have a clear decreasing trend in EM value over time. Also, the SLE craters in both Early (~1.2–3.4 Ga) and Middle-to-Late (<1.2 Ga) Amazonian respectively exhibit a trend with their EM values broadly decreasing with time. Resembling the case in SUIP (Figure 7), the results (Figure 8) again show that the EM values are not crater

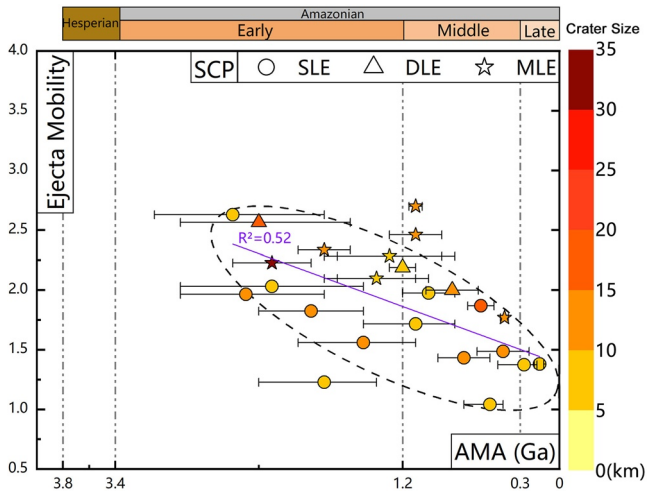

Figure 8. Scatter plot of the ejecta mobility (EM) values versus absolute model ages of the 24 layered ejecta craters (LECs) in southern Chryse Planitiaregion. The color variation from light yellow to deep red indicate LEC diameters with an increasing trend. The linear fitting results (the purple line) of the LECs within the dashed ellipse suggests a generally decreasing trend in average EM values with time, ranging from ~2.5 to 1.5.

size-dependent. In summary, if the three outliers are not included, a linear fit trend line (purple line in Figure 8) indicates the average EM values gradually decrease from ~2.5 to 1.5 in the past 3.0 Ga.

4.4. Crater Excavation Depth

The results show the excavation depths of most LECs in SUIP are concentrated between 600 and 1,500 m, and the youngest (late Amazonian, 0–0.3 Ga) are between 300 and 1,200 m (Figure 5). There is no clear excavation depth trend with time for SLE and DLE craters, whereas the MLE craters appear to have a significantly decreasing trend with time for both their diameters and excavation depths (Figure 5). Generally, the excavation depths for LECs in SCP display no trend in time and the majority suggest an average of ~1 km (Figure 6). However, the excavation depth for the youngest SLE (~0.2 Ga) is ~800 m and the shallowest depth is ~600 m for the SLE crater ~2.0 Ga in age. It should be noted that the shallowest excavation depths of the MLE craters in both SUIP and SCP are ~800 and 900 m (Figures 5 and 6), respectively.

5. Discussion

5.1. Model Age Analysis of LECs

Most of all studied LEC examples in both SUIP and SCP regions were dated to have formed throughout the Amazonian epoch, especially the early and middle Amazonian epoch, and only a few in the late Hesperian epoch (Figures 5 and 6). The lack of model ages for the Noachian and Hesperian is primarily due to the potential landing areas located in the northern lowlands. These lowlands zones are mainly covered by younger geological units (e.g., Av, AHv, lHl, lHt and Hto unit; Figure 3; Tanaka et al., 2014). Specifically, as a subset of the lowlands, most of the southern Utopia Planitia is covered by Vastitas Borealis Formation (VBF) formed in the late Hesperian (Tanaka et al., 2003; Werner & Tanaka, 2011). As an indicator marking the large-scale cessation of emplacement of the sedimentation in the northern lowlands, the VBF has been interpreted as resulting from either volatile expulsion from the compaction of a fluid-laden sedimentary unit (Salvatore & Christensen, 2014), or local periglacial processes acting on outflow channel sediments and other older plain materials (Tanaka et al., 2003), or sublimation residues (Kreslavsky & Head, 2002), or ocean sediments (Baker et al., 1991), or any combination of them. AMAs of the VBF in southern Utopia Planitia were found to be from ~3.5 to ~3.6 Ga (Ivanov et al., 2014). The superposition of LECs on the surface of the VBF units indicate that the LECs postdate the formation of the VBF. The relative age relationship is consistent with our CSFD dating results for the southern Utopia Planitia: the LECs on the VBF unit were aged younger than 3.4 Ga (see Table S1), relative to the older VBF units (~3.5–3.6 Ga, Ivanov et al., 2014). In addition, the post-impact basin evolution of Isidis Planitia is dominated by volcanism in the early Hesperian epoch (~3.8–3.5 Ga), subsequently followed by fluvial/glacial processes dominated period (~3.4–3.1 Ga) leading to repeated extensive surface resurfacing in the basin (Ivanov et al., 2012). Our dating results of the LECs within the basin (between ~1.1 Ga and ~2.9 Ga) are supportive of the relative age relationship within the framework of these surface processes in the Isidis Planitia.

The SCP is the convergent place of the circum-Chryse outflow channels (i.e., Kasei, Maja, Simud, Tiu, Ares, and Mawrth Valles). The main water activity phase to form these channels has been suggested to be between ~3.8 Ga and ~3.0 Ga, but might have undergone episodic pulses with lower activity into Amazonian (Baker & Kochel, 1979; Carr & Clow, 1981; Masursky et al., 1977). Records of early impact events (i.e., Noachian, and early Hesperian), therefore, might have been erased by later fluvial activities or covered by sediments emplaced from the highlands (Golombek et al., 1997), thus supporting a relatively younger age of the well-preserved LECs thereafter (between ~0.15 Ga and ~2.5 Ga; see Table S2) in SCP.

The CSFD dating technique has already been used to derive AMAs of LECs in SCP by Reiss et al. (2006), but their study is only focused on small and limited localities. Their results show that the LECs with ejecta eroded by fluvial events have AMAs ~3.8 Ga and between ~1.5 Ga and ~0.6 Ga for the LECs superposed by channels (Reiss et al., 2006; their Figure 10). In comparison, the absence of older (i.e., Hesperian and Noachian) LECs in

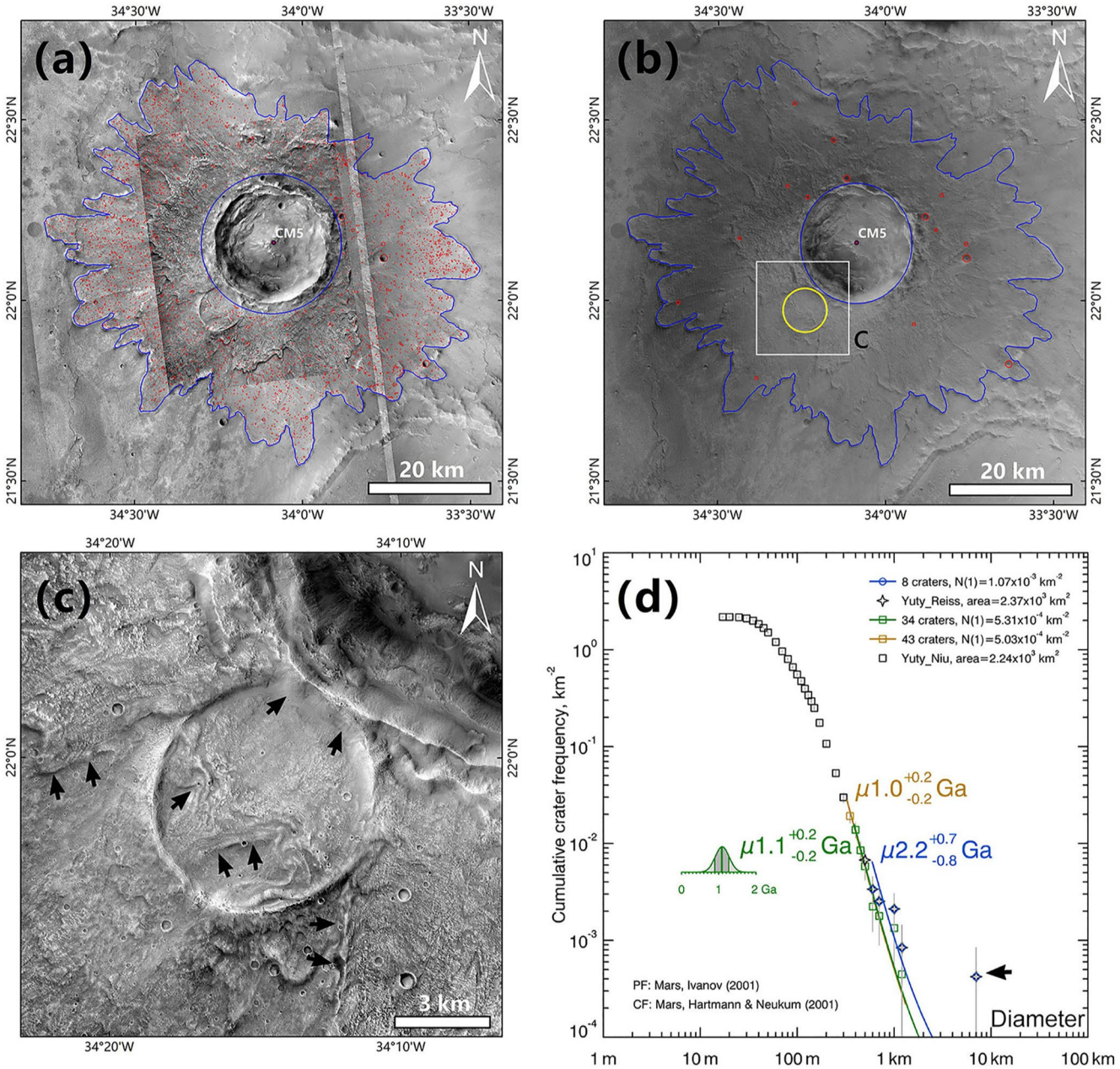

Figure 9. (a) Yuty Crater seen in Context Camera (CTX) mosaic with mapped crater count area (blue line) and identifiable superposed craters (red circles) in our study. (b) Yuty Crater seen in HRSC images with mapped crater count area (blue line) and identifiable superposed craters (D > 600 m) (red circles and a yellow circle) in Reiss's study (Reiss et al., 2006). (c) Enlarged view of the crater indicated by the white box in (b) from the CTX mosaic. The black arrows indicate evidence of ejecta burying, flowing, and bypassing the crater. (d) Dating results of the Yuty crater. Cumulative crater frequency plot showing production function (PF) fitted to the crater diameter range 0.4–1.3 km in our study, and the absolute model ages (AMA), $\mu 1.1^{+0.2}_{-0.2}$ Ga (Poisson timing analysis) (green squares) and $\mu 1.0^{+0.2}_{-0.2}$ Ga (cumulative fit) (orange squares). The PF fitted (blue circles) to the crater diameter range 0.6–8 km by Reiss et al. (2006), and the AMA, $\mu 2.2^{+0.7}_{-0.8}$ Ga (cumulative fit). The black arrow points to the crater shown in Figure 9c.

our SCP results is due to our exclusion of the LECs with ejecta deposits that have undergone obvious and significant degradation. The LEC (Figure 9a), named Yuty and labeled #CM5 in Figure 3b, was dated to be $\mu 1.0^{+0.2}_{-0.2}$ Ga (Figure 9d, marked in orange font) using the CF of Hartmann and Neukum (2001) and the PF of Ivanov (2001) with cumulative fit in our study, but an older model age $\mu 2.2^{+0.7}_{-0.8}$ Ga (Figure 9d, marked in blue font) using the same method was derived by Reiss et al. (2006) (their Figure 10). The difference may be caused by the following three factors. First, smaller superposed craters were recognized in our study by using the CTX images (5.0 m/pix;

Figure 9a) with a higher resolution than the HRSC images (12–15 m/pix; Figure 9b) used by Reiss et al. (2006). The identification of smaller craters used for dating indicates that their hosting ejecta appears to have not been affected by later geological processes, which makes our derived CSFD results more robust. Second, there is a subjective difference in identifying which craters are superposed on the ejecta. We are confident in our assessment that the noted crater in Figure 9b (the yellow circle) was formed before the ejecta emplacement based on their stratigraphic relationship: the crater is filled and covered with fluidized ejecta (Figure 9c), and if the crater formed later than the LEC, the sharpness of the LEC rim at the crater northeast edge should not have been well preserved. Thus, we argue that the crater should not be part of the CSFD. In addition, the derived model ages are greatly influenced by the diameter range of the PF fitting, which could also be subjective (Figure 9d).

5.2. Implications for Surface/Subsurface Ice Conditions

The formation of LECs is assumed (based upon multiple lines of evidence discussed earlier) to require surface (icy layer) and/or underground water/ice (i.e., ice-cemented regolith/rock or volatile-rich target) to be involved (e.g., Baloga et al., 2005; Barlow, 2005; Costard, 1989; Jones et al., 2016; Kuzmin, 1980; Kuzmin et al., 1988; Oberbeck, 2009; Weiss & Head, 2014). The DLE craters are thought to have formed through impact into a buried ice layer (e.g., Senft & Stewart, 2008) or a rock/ice mixture (e.g., Wulf & Kenkmann, 2015) or a surface ice layer (Weiss, 2019; Weiss & Head, 2013, 2018). The MLE craters have been interpreted as resulting from an impact into material below the ice-cemented cryosphere (or permafrost; Clifford, 1991), while the excavation depths of SLE craters are commonly considered to be limited within the upper ice-cemented cryosphere where ice fills the pore-space (e.g., Weiss & Head, 2017; their Figure 2). The varying thickness of the icy substrate and the related subsurface concentrations (Boynton et al., 2002) at the time of impact are hypothesized to highly affect the EM value of the ejecta (e.g., Barlow, 2005; Costard, 1989; Weiss & Head, 2014). Thus, the relationship between EM values and ages of LECs might reflect the variation trend of subsurface volatiles concentrations over time (Barlow, 2004).

The average EM values of the SLE craters (all concentrated between 1.0 and 2.0; Figure 7) in SUIP region has not significantly changed in the past 3.5 Gyr, and this is consistent with the conclusion obtained by Barlow (2004). They used multiple characteristics, including relative crater depth, rim sharpness, ejecta blanket preservation, interior feature preservation, and thermal inertia to determine the relative ages of LECs ($D \geq 5$ km) between $\pm$ 30°N latitude and 0–180°W. Their results indicate that subsurface volatiles concentration remained almost stable at depth (>700 m) with time (Barlow, 2004). Though the secular diffusive loss of ice from the subsurface with time is inferred (Clifford & Hillel, 1983; Fanale et al., 1986; Mellon et al., 1997), volatile discharge and recharge, which are dominated by obliquity variations (Fanale et al., 1986; Mellon & Jakosky, 1995), have also greatly affected the dynamic evolution of the Martian cryosphere (Clifford, 1991; Weiss & Head, 2017). Water ice was delivered to and likely accumulated toward lower latitudes during the periods when Mars had relatively high obliquity (Head et al., 2003; Jakosky & Carr, 1985; Madeleine et al., 2009, 2014; Weiss, 2019). However, numerical models (e.g., Grimm et al., 2017) suggest that volatile distribution at depths larger than ~100 m would be stable and not affected by long-term obliquity variations. Further, thermal and molecular diffusion models analysis concluded that subsurface volatiles deeper than ~2 m should not be affected by the diurnal, seasonal, or long-term temperature variations over at least the past 2.5×10^6 yrs (Mellon & Jakosky, 1995).

The simple crater diameter/depth relations from Melosh (1989) suggest that our smallest LECs ($D \approx 4$ km) would have excavated to depths greater than 400 m, well into, and maybe under, the estimated Hesperian-Amazonian stable layer of volatile concentration (~100 m and deeper) which is not affected by Mars obliquity and temperature variations (Grimm et al., 2017). The narrow EM value range between 1.0 and 2.0 for the SLE craters in SUIP does not show obvious trend on the geological time scales (Figure 7). Results of this analysis combined with numerical models (Grimm et al., 2017; Mellon & Jakosky, 1995) suggest that subsurface volatile concentrations might have been relatively stable over at least the past 3.5 Gyr in the SUIP region at the depth excavated by the studied craters. A smaller LEC ($D \approx 7$ km; Figure 10a, #US21) shows an AMA up to $\mu 52^{+20}_{-10}$ Ma (Figure 10c) suggesting that subsurface water ice likely persists to present at depth ~700 m in the southern Utopia Planitia. In fact, the depth to the subsurface-ice table calculated by the Melosh (1989) theoretical considerations is a lower boundary, because a certain percentage of volatile substances must have been excavated before the final emplacement of the fluidized ejecta deposits (Costard & Kargel, 1995). Experimental and numerical simulations have suggested critical volatile concentrations of 16%–60% involved (Senft & Stewart, 2008; Wohletz &

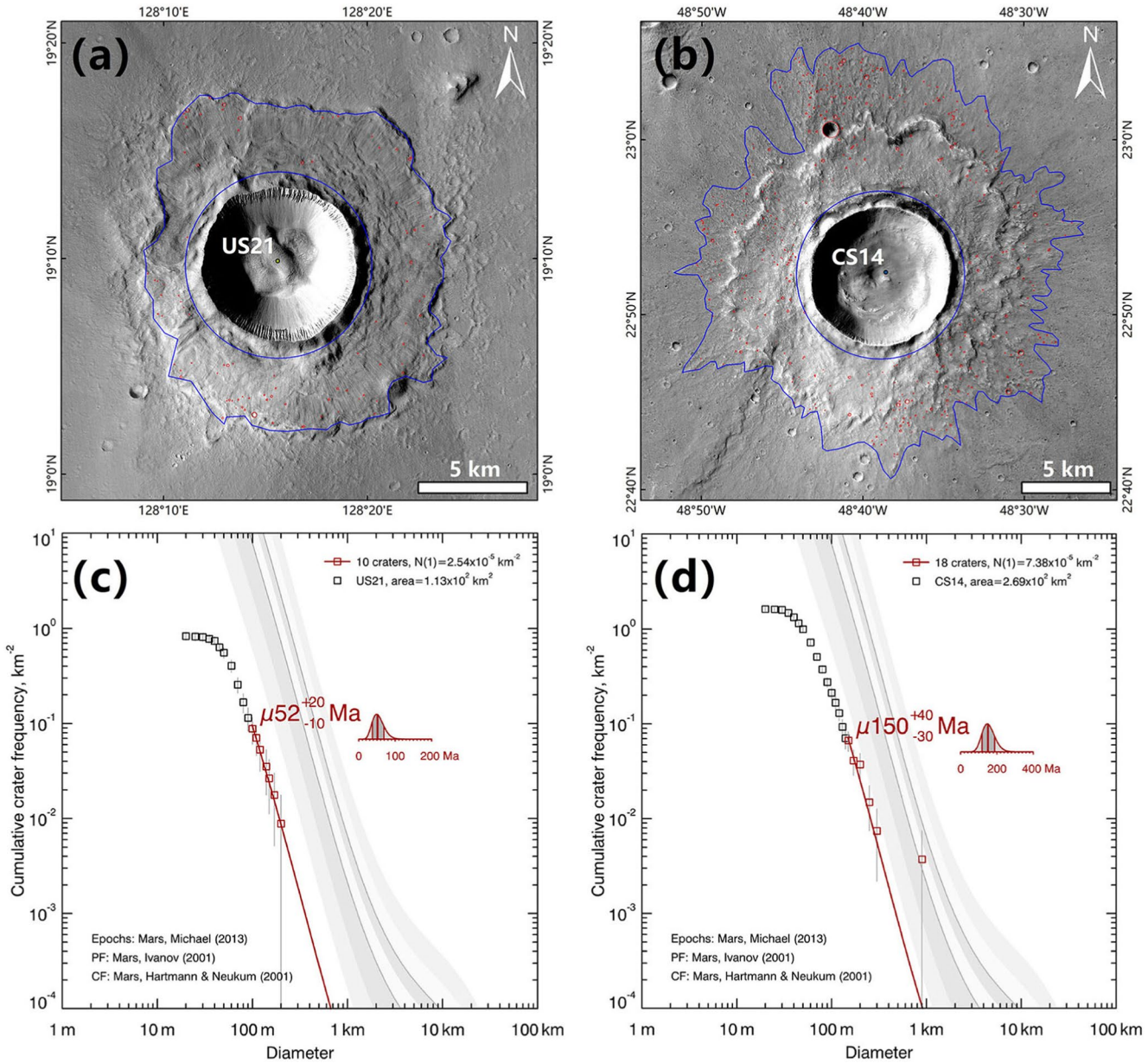

Figure 10. (a) A relatively young ($\mu 52^{+20}_{-20}$ Ma), smaller diameter layered ejecta crater (LEC) (#US21) in SUIP region with mapped crater count area (between blue lines) and identifiable superposed craters (red circles). (b) A relatively young ($\mu 150^{+40}_{-30}$ Ma), smaller diameter LEC (#CS14) in southern Chryse Planitia region with mapped crater count area (blue line) and identifiable superposed craters (red circles). (c) Dating results of the #US21 LEC. (d) Dating results of the #CS14 LEC.

Sheridan, 1983; Woronow, 1981). Therefore, the present subsurface water ice depth may be less than ~700 m in the southern Utopia Planitia. Since there are few LECs (including six SLE and two MLE craters, Figure 3a; AMAs between ~1.1 Ga and ~2.9 Ga) identified in the Isidis Planitia, the present depth of subsurface ice cannot be estimated there with any confidence.

Geomorphologic evidence also suggests that the SUIP region may have undergone a long "dry" history since Hesperian epoch. For example, craters with pancake-like ejecta are also thought to result from impacts into target materials containing ice/water (Ivanov et al., 2014 and references therein). Relative to smaller pancake-like craters, larger LECs in Utopia Planitia tend to occur at the periphery of the basin and this is likely explained by less ice/water concentration at the high-topography basin edge than in the lower center (Ivanov et al., 2014). Further, sublimation rate of subsurface ice/water would have been greatly decreased by being covered with a

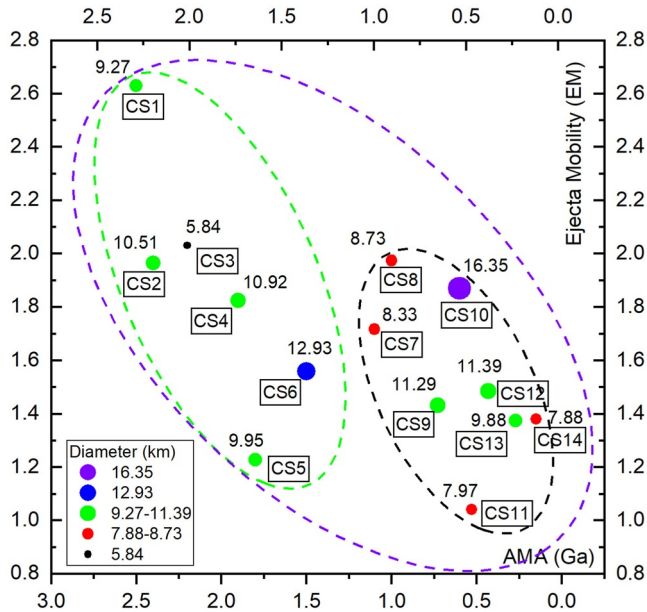

Figure 11. The scatter plot of ejecta mobility (EM) values of the 14 single layered ejecta (SLE) craters in southern Chryse Planitia. The symbol size varies by crater diameter (the larger the bubble, the larger the crater size). At the same, the exact value of diameter of each SLC crater is marked above each bubble, while the names of individual SLE craters are given below bubbles with black borders. The general decreasing trend of EM variation of these SLE craters is illustrated by the violet-color dashed ellipse. The black- and green-color dashed ellipses indicate the Middle-to-Late (<1.2 Ga) and Early Amazonian-aged (~1.2–3.4 Ga) SLE craters, respectively. Their areal distribution and locations are shown in Figure 12.

surficial debris layer (even a few meters thick would effectively decrease sublimation; Carr & Head, 2003; Farmer & Doms, 1979), which is evidenced by the presence of VBF formed in the Hesperian (Tanaka et al., 2003; Werner & Tanaka, 2011). Thus, the basin-edge, high-topography SUIP may be able to maintain a relatively stable water/ice concentration or cryosphere at a certain depth in the interior, which is further favored by our observational results displaying a steady status of EM values fluctuating between 1.0 and 2.0 for SLEs since Hesperian in SUIP (Figure 7).

In SCP, the linear fitting line of the average EM values of LECs shows a positive linear correlation (Figure 8), suggesting an overall decreasing-trend of the concentration of subsurface volatiles over time (older LECs exhibit high EM values, while younger LECs exhibit low EM values). This means that the depth of the subsurface ice table gradually increases over time or volatile concentration decreases or both, seeming to be somewhat consistent with the results obtained by Reiss et al. (2006). We also note that the general trend observed with SLE craters in Figure 8 is based on the ensemble of craters. There are individual craters of similar size but dissimilar age that follow this general trend of decreasing EM values toward younger ages (e.g., ~11-km-diameter SLE craters CS2, CS4, and CS9 with EM values and ages of [1.96, 2.4 Ga], [1.82, 1.9 Ga], and [1.43, 0.73 Ga], respectively; Figure 11), but a few similar-sized craters do not follow this EM-age inverse trend (e.g., LEC craters CS11 and CS14 (7.97 vs. 7.88 km) with EM values and ages of [1.04, 0.53 Ga] and [1.37, 0.15 Ga]; Figure 11). The SLE crater CS14 is located in the southwestern border area of the Chryse basin with higher topography (Figure 12), while CS11 in the lower channel floor near the Ares channel outlet. The higher topography may have lower temperatures to maintain the subsurface volatiles stable for a long time, but the channel interior would be an ideal negative place for weathering materials to fill in and deposit, thus causing an upper dry layer of increasing thickness with time. Consequently, this special depositional setting might have resulted in a relatively lower volatile content for CS11's ejecta. Thus, the above analysis suggests that different geological settings will exert a certain influence on the final appearance of ejecta blankets of LECs, increasing the complexity of interpreting subsurface volatile conditions. These interpretations are consistent with and again confirmed previous conclusions that volatile concentrations vary with locality (e.g., Barlow, 2004; Costard, 1989). However, given that EM is a normalized, dimensionless parameter, the general downward trend of subsurface volatile concentrations for SCP was thus inferred from the entire population of all the investigated LECs (Figure 8) and the 14 SLE craters (Figure 11), not a very limited subset.

Smaller LECs (D < 3 km) in the SCP region are relatively absent, suggesting that near-surface ground ice was lost over time in the Amazonian epoch. A lowering of the subsurface ice table due to loss of volatiles possibly occurred after the last large-scale groundwater recharge, which coincides with the main activity phase (between ~3.8 Ga and ~3.0 Ga) of the circum-Chryse outflow channels (Baker & Kochel, 1979; Carr & Clow, 1981; Masursky et al., 1977). Generally, compared with high latitudes, the equatorial regions such as SCP should have experienced a relatively continuous loss of subsurface ice throughout the Mars geological history (Clifford, 1993; Clifford & Hillel, 1983; Fanale et al., 1986). However, the EM variation of the SLE craters in SCP appears to have an abrupt change in trend at around 1.2 Ga (Figure 11), which may indicate that the area had been recharged by small-scale periodic flood events at the time (Carr & Head, 2010; Marchenko et al., 1998; Neukum & Hiller, 1981; Warner et al., 2009). The shallow subsurface ice table, however, might not be sufficiently stable to remain for longer times from small-scale flooding. Most of the SLE craters potentially younger than 1.2 Ga are located near the terminal ends (dashed black polygons in Figure 12) of the channels originating from the southern highlands with higher topography. This boundary zone, where the channels run into the northern lowland, is a place susceptible to resurfacing or erosion by periodic flooding and/or mass-wasting events. This could explain why these Late Amazonian aged SLE craters (CS7-CS14, Figures 11 and 12) with well-preserved fluidized ejecta blankets tend to distribute closer to the north-south hemisphere boundary, in particular to the outlet area

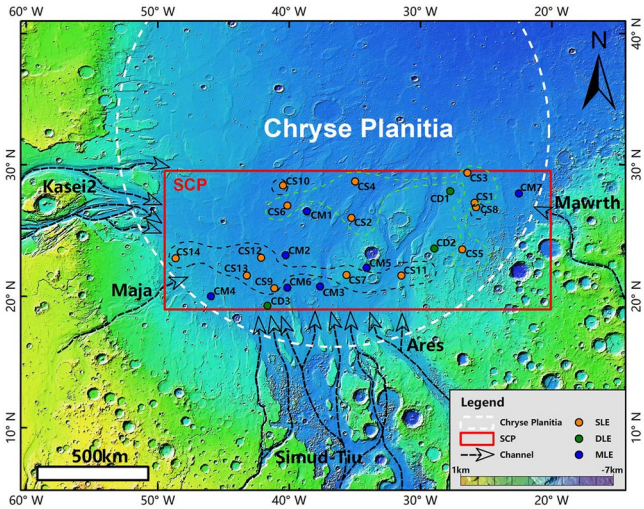

Figure 12. Areal distribution of the studied layered ejecta craters in southern Chryse Planitia (SCP). The single layered ejecta (SLE) craters potentially younger than 1.2 Ga, outlined by the black dashed lines (also see Figure 11), tend to be located in the regions near the outlet areas of the channels sourced from the surrounding highlands. The average ejecta mobility values for the Middle-to-Late (<1.2 Ga; black dashed lines) and Early Amazonian-aged (~1.2–3.4 Ga; green dashed line) SLE craters show a general decreasing trend with time (indicated by the black and green dashed ellipses in Figure 11, respectively), consistent with the general downward trend of subsurface volatile concentrations over time in SCP, inferred from all the 14 investigated SLE craters (Figure 11) and the 21 SLE and direct layered ejecta craters (black dashed ellipse, Figure 8).

of highland channels. Additionally, the correspondence of some shallower excavation depths to younger LEC ages ($\mu 150^{+40}_{-30}$ Ma, D ≈ 8 km; Figures 10b and 10d, #CS14) seems to indicate that subsurface ice most likely still exists and the depth is ~800 m in SCP (Figure 6).

In summary, the average EM values of the two candidate landing areas have different trends over time, and this may suggest that the evolutionary history of subsurface volatiles in the two regions is different. The dry regolith (above the ice-cemented cryosphere) is predicted to be several tens to hundred meters thick at the equator, but its thickness decreases toward high latitudes (Weiss & Head, 2017 and references therein). The thickness of the upper dry regolith layer varies along with several more major or minor factors: local surface temperature conditions, atmospheric humidity, geothermal gradient, porosity, and thermal diffusive properties of the regolith (e.g., Fanale et al., 1986; Grimm et al., 2017; Grimm & Painter, 2009; Mellon et al., 1997). Among them, the local mean annual surface temperature is mainly a function of latitude and obliquity. Based on the EM variation of SLE craters, subsurface volatile concentrations may have been relatively stable over at least the past 3.5 Ga in SUIP (Figure 7), whereas our results show a decreasing-trend of the concentration of subsurface volatiles over time in SCP in the past 2.5 Ga (Figure 8). This suggests that the tempo-spatial variation of subsurface water ice concentrations in SCP has a more substantial change than that in SUIP, which may be due to the SCP being closer to the equator.

LECs with a diameter of less than 3 km are not recorded within the existing databases (Li et al., 2015; Robbins & Hynek, 2012). Some previous efforts have been made to identify smaller LECs (e.g., Reiss et al., 2005, 2006). With the high-resolution images (CTX, 5.0 m/pix) of Mars becoming available, some much smaller LECs (D ≤ 1.5 km) have been identified (e.g., Kirchoff & Grimm, 2018 and this study). Following the simple crater scaling relations (Melosh, 1989), the excavation depth is 150 m or less suggesting that local ground ice was likely shallower than 150 m when the impact occurred. Because the areas of ejecta blanket deposits of these LECs are too small to measure small, superposed craters, their model ages cannot currently be robustly estimated.

5.3. Recommendations for Tianwen-1 and Future Exploration and Analysis

The location of the landing site of the Tianwen-1 lander and Zhurong rover is marked in Figure 3a (red star). The Tianwen-1 landing site is near to the crater UM5 investigated is this study, and this area is found to be distributed with a series of sedimentary and volcanic materials and features (Mills et al., 2021; X. Wu, Liu, et al., 2021). The sequence of events to form the geomorphic features and units has been approximately estimated by their apparent spatial relationships (Mills et al., 2021), but this proposed stratigraphy needs to be further tested and validated in future crater-counting and in-situ exploration studies, in particular, from robotic sample return missions.

A significantly striking difference between the landing-site-containing SUIP and SCP is that the SUIP region might have been highly affected by the magmatic and volcanic activities associated with Elysium Mons to its east and Syrtis Major Planum to the west of Isidis Planitia (Figure 2). This can be inferred from numerous pitted cones in both Utopia and Isidis planitia, which have been interpreted as resulting from sedimentary volcanism or volcanic in origin (e.g., Ghent et al., 2012; Ivanov et al., 2014; McGowan, 2011; Skinner Jr. & Tanaka, 2007). If the hypothesis of sedimentary or mud volcanism (McGowan, 2011; Skinner Jr. & Tanaka, 2007) is right, the pitted cone-forming materials should have sourced from a pressurized subsurface reservoir containing volatiles. Checking the compositional information of both pitted cones and ejecta deposits of LECs might bring a confirmation of whether a same subsurface volatile-containing reservoir was shared by them. The landing site of Tianwen-1 lander and Zhurong rover is near to a pitted cone to its northwest (Mills et al., 2021; their Figure 4) and the LEC UM5 (Figure 3a) investigated in this study. Therefore, high-resolution and detailed spectral mapping of the pitted cone and the multiple-layer ejecta crater would address this issue. At present, the Zhurong rover is traveling south for specific in situ survey of a series of geologic features and subsurface structures along

its path. Particularly, the pitted cones in the distance have been chosen as an important investigation target (Liu et al., 2021). Besides, there will also be a chance for a visit to the LEC at the south end of the landing area (Liu et al., 2021). Thus, Zhurong rover could carry out field investigations of both features, searching for definitive evidence of compositional similarities and differences and feature origins.

The depths and detailed profile conditions of subsurface volatile-containing layers can be investigated directly from radar detections. The Mars Orbiter Scientific Investigation Radar (MOSIR) and Rover Ground-Penetrating Radar (GPR) onboard Tianwen-1 rover has the capability to explore the subsurface properties to depths up to 100 m in the crust depending on subsurface terrain properties (Fan et al., 2021; Zou et al., 2021). The GPR is designed to characterize the subsurface layers distribution, properties, and their thicknesses. It contains two radar channels which operate in the frequency range 15–95 MHz and 0.45–2.15 MHz, respectively. The lower frequency channel will penetrate the substrate to depths of 10–100 m with a resolution of a few meters, while the higher frequency channel will be able to penetrate 3–10 m with a resolution of a few centimeters (Zhou et al., 2020). The existence of a series of geomorphic features with their origins involving water-related activities (e.g., Ivanov et al., 2014; Mills et al., 2021; X. Wu, Liu, et al., 2021) in the Tianwen-1 landing site provides good testing targets for exploration of the subsurface water ice conditions by the rover, which are key to understanding Mars' climate and geologic history.

6. Conclusions

In this study, we carried out the stratigraphic, morphologic, and morphometric analysis of 68 LECs, which are located in the two candidate landing areas of China's first Mars exploration mission. We determined the AMAs of the LECs, measured their EM values, and estimated their excavation depths to analyze the evolutionary history of regional subsurface volatile concentrations. The 41 LECs in the SUIP were dated to have formed throughout the Amazonian epoch (~3.4 Ga to present), and only three in the Hesperian epoch (~3.4–3.8 Ga). However, all the studied 24 LECs in SCP show AMAs of <2.5 Ga, Amazonian in age. We found that the EM variation of LECs have different trends over time in the two regions: the EM values of LECs show no significant regular change over time in SUIP, whereas the EM values seem to decrease over time in SCP. The results are consistent with historic periods of fluvial activity in SCP resulting in episodic resurfacing and recharge of volatiles, especially in the channels' outlet areas where only relatively younger LECs are observed in this study. As a contrast, the volatile concentrations might have not changed much in SUIP. The results lead us to conclude that the evolution history of the concentration of subsurface volatiles varies with locality on Mars.

We further estimated the depth of underground ice based on the excavation depths of younger LECs. The results show that a layer of subsurface water/ice with a depth of ~700 m may have been present in SUIP, and a depth of ~800 m is inferred for the SCP. The current depth of underground ice may reflect the long-term dehydration of the ice-cemented regolith/rock in the upper several hundred meters. The presence of newly identified LECs $\leq$ 1.5 km may suggest that the ice depth may be locally less than 150 m in some areas, favoring the previous estimates of substantial local variations in cryosphere thickness (e.g., Clifford et al., 2010; Weiss & Head, 2017). The search for subsurface water ice on Mars is the objective of both the MOSIR and Mars Rover Penetrating Radar (RoPeR) onboard the Tianwen-1 mission, which have a potential to penetrate a depth up to 100 m and may bring exciting discoveries. We also concluded with recommendations for Tianwen-1 and future exploration and analysis that could help test and validate the proposed hypotheses for the origins of a series of geologic features and martian geological evolution history at regional and globle scales.

Conflict of Interest

The authors declare no conflicts of interest relevant to this study.

Data Availability Statement

For all 68 LECs (44 in SUIP and 24 in SCP), the CSFD-based dating plots, the CTX mosaic displaying their ejecta deposits outline (blue line) and identifiable superposed craters (red circles), the resulting SCC files (used for dating) for individual LECs exported from ArcGIS with the “Crater Tools”, and the geologic maps shown in

Figure 3 and arranged in ArcGIS version can be found online (S. Niu et al., 2021, Zenodo, https://doi.org/10.5281/zenodo.5108950).

Acknowledgments
This research was funded by the Strategic Priority Program of the Chinese Academy of Sciences (XDB41000000), the Science and Technology Development Fund, Macau SAR (0049/2020/A1), the National Natural Science Foundation of China (11903090 and 42172265), the pre-research project on Civil Aerospace Technologies (No. D020104) funded by China's National Space Administration, and the National Key Research and Development Program of China (2021YFA0716100). We are grateful to Michelle Kirchoff and an anonymous reviewer for their thoughtful and constructive reviews and those from the Editor Bradley J. Thomson, which greatly helped improve the quality of the manuscript.

References

Baker, V. R., & Kochel, R. C. (1979). Martian channel morphology: Maja and Kasei valles. *Journal of Geophysical Research: Solid Earth*, *84*(B14), 7961–7983. https://doi.org/10.1029/jb084ib14p07961

Baker, V. R., Strom, R. G., Gulick, V. C., Kargel, J. S., Komatsu, G., & Kale, V. S. (1991). Ancient oceans, ice sheets and the hydrological cycle on Mars. *Nature*, *352*(6336), 589–594. https://doi.org/10.1038/352589a0

Baloga, S. M., Fagents, S. A., & Mouginis-Mark, P. J. (2005). Emplacement of Martian rampart crater deposits. *Journal of Geophysical Research: Planets*, *110*(E10), E10001. https://doi.org/10.1029/2004je002338

Bandfield, J. L. (2007). High-resolution subsurface water-ice distributions on Mars. *Nature*, *447*(7140), 64–67. https://doi.org/10.1038/nature05781

Barlow, N. G. (2004). Martian subsurface volatile concentrations as a function of time: Clues from layered ejecta craters. *Geophysical Research Letters*, *31*(5), L05703. https://doi.org/10.1029/2003gl019075

Barlow, N. G. (2005). A review of Martian impact crater ejecta structures and their implications for target properties. *Large meteorite impacts III*, *384*, 433–442. https://doi.org/10.1130/0-8137-2384-1.433

Barlow, N. G. (2006). Impact craters in the northern hemisphere of Mars: Layered ejecta and central pit characteristics. *Meteoritics & Planetary Sciences*, *41*(10), 1425–1436. https://doi.org/10.1111/j.1945-5100.2006.tb00427.x

Barlow, N. G. (2015). Characteristics of impact craters in the northern hemisphere of Mars. In *Large Meteorite Impacts and Planetary Evolution IV* (Vol. 518, pp. 31–63). Geological Society of America. https://doi.org/10.1130/2015.2518(03)

Barlow, N. G., Boyce, J. M., & Cornwall, C. (2014). Martian Low-Aspect-Ratio Layered Ejecta (LARLE) craters: Distribution, characteristics, and relationship to pedestal craters. *Icarus*, *239*, 186–200. https://doi.org/10.1016/j.icarus.2014.05.037

Barlow, N. G., Boyce, J. M., Costard, F. M., Craddock, R. A., Garvin, J. B., Sakimoto, S. E., et al. (2000). Standardizing the nomenclature of Martian impact crater ejecta morphologies. *Journal of Geophysical Research*, *105*(E11), 26733–26738. https://doi.org/10.1029/2000je001258

Barlow, N. G., & Bradley, T. L. (1990). Martian impact craters: Correlations of ejecta and interior morphologies with diameter, latitude, and terrain. *Icarus*, *87*(1), 156–179. https://doi.org/10.1016/0019-1035(90)90026-6

Barlow, N. G., Koroshetz, J., & Dohm, J. M. (2001). Variations in the onset diameter for Martian layered ejecta morphologies and their implications for subsurface volatile reservoirs. *Geophysical Research Letters*, *28*(16), 3095–3098. https://doi.org/10.1029/2000gl012804

Barlow, N. G., & Perez, C. B. (2003). Martian impact crater ejecta morphologies as indicators of the distribution of subsurface volatiles. *Journal of Geophysical Research*, *108*(E8), 5085. https://doi.org/10.1029/2002je002036

Barnouin-Jha, O. S., Baloga, S., & Glaze, L. (2005). Comparing landslides to fluidized crater ejecta on Mars. *Journal of Geophysical Research*, *110*(E4), E04010. https://doi.org/10.1029/2003JE002214

Barnouin-Jha, O. S., & Schultz, P. H. (1998). Lobateness of impact ejecta deposits from atmospheric interactions. *Journal of Geophysical Research*, *103*(E11), 25739–25756. https://doi.org/10.1029/98JE02025

Black, B. A., & Stewart, S. T. (2008). Excess ejecta craters record episodic ice-rich layers at middle latitudes on Mars. *Journal of Geophysical Research*, *113*(E2), E02015. https://doi.org/10.1029/2007je002888

Boyce, J., Barlow, N., Mouginis-Mark, P., & Stewart, S. (2010). Rampart craters on Ganymede: Their implications for fluidized ejecta emplacement. *Meteoritics & Planetary Sciences*, *45*(4), 638–661. https://doi.org/10.1111/j.1945-5100.2010.01044.x

Boyce, J. M., & Mouginis-Mark, P. J. (2006). Martian craters viewed by the Thermal Emission Imaging System instrument: Double-layered ejecta craters. *Journal of Geophysical Research*, *111*(E10), E10005. https://doi.org/10.1029/2005je002638

Boyce, J. M., Wilson, L., & Barlow, N. G. (2015). Origin of the outer layer of martian low-aspect ratio layered ejecta craters. *Icarus*, *245*, 263–272. https://doi.org/10.1016/j.icarus.2014.07.032

Boynton, W. V., Feldman, W. C., Squyres, S. W., Prettyman, T. H., Brückner, J., Evans, L. G., et al. (2002). Distribution of hydrogen in the near surface of Mars: Evidence for subsurface ice deposits. *Science*, *297*(5578), 81–85. https://doi.org/10.1126/science.1073722

Buczkowski, D. L., & McGill, G. E. (2002). Topography within circular grabens: Implications for polygon origin, Utopia Planitia, Mars. *Geophysical Research Letters*, *29*(7), 59-1–59-4. https://doi.org/10.1029/2001gl014100

Carr, M. H. (1996). *Water on Mars* (p. 229). Oxford University Press. https://doi.org/10.1016/b978-075069707-1/50056-0

Carr, M. H., & Clow, G. D. (1981). Martian channels and valleys: Their characteristics, distribution, and age. *Icarus*, *48*(1), 91–117. https://doi.org/10.1016/0019-1035(81)90156-1

Carr, M. H., Crumpler, L. S., Cutts, J. A., Greeley, R., Guest, J. E., & Masursky, H. (1977). Martian impact craters and emplacement of ejecta by surface flow. *Journal of Geophysical Research*, *82*(28), 4055–4065. https://doi.org/10.1029/js082i028p04055

Carr, M. H., & Head, J. W., III. (2003). Oceans on Mars: An assessment of the observational evidence and possible fate. *Journal of Geophysical Research*, *108*(E5), 5042. https://doi.org/10.1029/2002JE001963

Carr, M. H., & Head, J. W., III. (2010). Geologic history of Mars. *Earth and Planetary Science Letters*, *294*(3–4), 185–203. https://doi.org/10.1016/j.epsl.2009.06.042

Christensen, P. R., Jakosky, B. M., Kieffer, H. H., Malin, M. C., McSween, H. Y., Nealson, K., et al. (2004). The thermal emission imaging system (THEMIS) for the Mars 2001 Odyssey Mission. *Space Science Reviews*, *110*(1), 85–130. https://doi.org/10.1007/978-0-306-48600-5_3

Clifford, S. M. (1991). The role of thermal vapor diffusion in the subsurface hydrologic evolution of Mars. *Geophysical Research Letters*, *18*(11), 2055–2058. https://doi.org/10.1029/91gl02469

Clifford, S. M. (1993). A model for the hydrologic and climatic behavior of water on Mars. *Journal of Geophysical Research*, *98*(E6), 10973–11016. https://doi.org/10.1029/93je00225

Clifford, S. M., & Hillel, D. (1983). The stability of ground ice in the equatorial region of Mars. *Journal of Geophysical Research*, *88*(B3), 2456–2474. https://doi.org/10.1029/jb088ib03p02456

Clifford, S. M., Lasue, J., Heggy, E., Boisson, J., McGovern, P., & Max, M. D. (2010). Depth of the Martian cryosphere: Revised estimates and implications for the existence and detection of subpermafrost groundwater. *Journal of Geophysical Research*, *115*, E07001. https://doi.org/10.1029/2009JE003462

Costard, F. M. (1989). The spatial distribution of volatiles in the Martian hydrolithosphere. *Earth, Moon, and Planets*, *45*(3), 265–290. https://doi.org/10.1007/bf00057747

Costard, F. M., & Kargel, J. S. (1995). Outwash plains and thermokarst on Mars. *Icarus*, *114*(1), 93–112. https://doi.org/10.1006/icar.1995.1046

Croft, S. K. (1985). The scaling of complex craters. *Journal of Geophysical Research*, *90*(S02), C828–C842. https://doi.org/10.1029/JB090iS02p0C828

Crumpler, L. S., & Tanaka, K. L. (2003). Geology and MER target site characteristics along the southern rim of Isidis Planitia, Mars. *Journal of Geophysical Research: Planets*, *108*(E12), 8080. https://doi.org/10.1029/2002je002040

Demura, H., & Kurita, K. (1998). A shallow volatile layer at Chryse Planitia, Mars. *Earth Planets and Space*, *50*(5), 423–429. https://doi.org/10.1186/bf03352129

Di Achille, G., & Hynek, B. M. (2010). Ancient ocean on Mars supported by global distribution of deltas and valleys. *Nature Geoscience*, *3*(7), 459–463. https://doi.org/10.1038/ngeo891

Edwards, C. S., Nowicki, K. J., Christensen, P. R., Hill, J., Gorelick, N., & Murray, K. (2011). Mosaicking of global planetary image datasets: 1. Techniques and data processing for thermal emission imaging system (THEMIS) multi-spectral data. *Journal of Geophysical Research*, *116*(E10), E10008. https://doi.org/10.1029/2010je003755

Erkeling, G., Reiss, D., Hiesinger, H., Ivanov, M. A., Hauber, E., & Bernhardt, H. (2014). Landscape formation at the Deuteronilus contact in southern Isidis Planitia, Mars: Implications for an Isidis Sea? *Icarus*, *242*, 329–351. https://doi.org/10.1016/j.icarus.2014.08.015

Erkeling, G., Reiss, D., Hiesinger, H., Poulet, F., Carter, J., Ivanov, M. A., et al. (2012). Valleys, paleolakes and possible shorelines at the Libya Montes/Isidis boundary: Implications for the hydrologic evolution of Mars. *Icarus*, *219*(1), 393–413. https://doi.org/10.1016/j.icarus.2012.03.012

Fan, M., Lyu, P., Su, Y., Du, K., Zhang, Q., Zhang, Z., et al. (2021). The Mars orbiter subsurface investigation radar (MOSIR) on China's Tianwen-1 mission. *Space Science Reviews*, *217*(1), 1–17. https://doi.org/10.1007/s11214-020-00786-4

Fanale, F. P., Salvail, J. R., Zent, A. P., & Postawko, S. E. (1986). Global distribution and migration of subsurface ice on Mars. *Icarus*, *67*(1), 1–18. https://doi.org/10.1016/0019-1035(86)90170-3

Farmer, C. B., & Doms, P. E. (1979). Global seasonal variation of water vapor on Mars and the implications for permafrost. *Journal of Geophysical Research*, *84*(B6), 2881–2888. https://doi.org/10.1029/JB084iB06p02881

Feldman, W. C., Prettyman, T. H., Maurice, S., Plaut, J. J., Bish, D. L., Vaniman, D. T., et al. (2004). Global distribution of near-surface hydrogen on Mars. *Journal of Geophysical Research*, *109*(E9), E09006. https://doi.org/10.1029/2003je002160

Ghent, R. R., Anderson, S. W., & Pithawala, T. M. (2012). The formation of small cones in Isidis Planitia, Mars through mobilization of pyroclastic surge deposits. *Icarus*, *217*(1), 169–183. https://doi.org/10.1016/j.icarus.2011.10.018

Golombek, M. P., Cook, R. A., Moore, H. J., & Parker, T. J. (1997). Selection of the Mars pathfinder landing site. *Journal of Geophysical Research*, *102*(E2), 3967–3988. https://doi.org/10.1029/96je03318

Greeley, R., Theilig, E., Guest, J. E., Carr, M. H., Masursky, H., & Cutts, J. A. (1977). Geology of Chryse Planitia. *Journal of Geophysical Research*, *82*(28), 4093–4109. https://doi.org/10.1029/js082i028p04093

Grimm, R. E., Harrison, K. P., Stillman, D. E., & Kirchoff, M. R. (2017). On the secular retention of ground water and ice on Mars. *Journal of Geophysical Research: Planets*, *122*(1), 94–109. https://doi.org/10.1002/2016je005132

Grimm, R. E., & Painter, S. L. (2009). On the secular evolution of groundwater on Mars. *Geophysical Research Letters*, *36*(24), L24803. https://doi.org/10.1029/2009gl041018

Grizzaffi, P., & Schultz, P. H. (1989). Isidis basin: Site of ancient volatile-rich debris layer. *Icarus*, *77*(2), 358–381. https://doi.org/10.1016/0019-1035(89)90094-8

Guidat, T., Pochat, S., Bourgeois, O., & Souček, O. (2015). Landform assemblage in Isidis Planitia, Mars: Evidence for a 3 Ga old polythermal ice sheet. *Earth and Planetary Science Letters*, *411*, 253–267. https://doi.org/10.1016/j.epsl.2014.12.002

Hartmann, W. K., & Neukum, G. (2001). Cratering chronology and the evolution of Mars. *Chronology and evolution of Mars*, 165–194. https://doi.org/10.1007/978-94-017-1035-0_6

Head, J. W., Hiesinger, H., Ivanov, M. A., Kreslavsky, M. A., Pratt, S., & Thomson, B. J. (1999). Possible ancient oceans on Mars: Evidence from Mars orbiter laser altimeter data. *Science*, *286*(5447), 2134–2137. https://doi.org/10.1126/science.286.5447.2134

Head, J. W., Kreslavsky, M. A., & Pratt, S. (2002). Northern lowlands of Mars: Evidence for widespread volcanic flooding and tectonic deformation in the Hesperian Period. *Journal of Geophysical Research: Planets*, *107*(E1), 3-1–3-29. https://doi.org/10.1029/2000je001445

Head, J. W., Mustard, J. F., Kreslavsky, M. A., Milliken, R. E., & Marchant, D. R. (2003). Recent ice ages on Mars. *Nature*, *426*(6968), 797–802. https://doi.org/10.1038/nature02114

Head, J. W., & Roth, R. (1976). Mars pedestal crater escarpments: Evidence for ejecta-related emplacement. In *Planetary cratering mechanics* (Vol. 259, p. 50).

Hiesinger, H., & Head, J. W., III. (2000). Characteristics and origin of polygonal terrain in southern Utopia Planitia, Mars: Results from Mars orbiter laser altimeter and Mars orbiter camera data. *Journal of Geophysical Research*, *105*(E5), 11999–12022. https://doi.org/10.1029/1999je001193

Ivanov, B. A. (2001). Mars/Moon cratering rate ratio estimates. *Space Science Reviews*, *96*(1), 87–104. https://doi.org/10.1007/978-94-017-1035-0_4

Ivanov, M. A., & Head, J. W. (2001). Chryse Planitia, Mars: Topographic configuration, outflow channel continuity and sequence, and tests for hypothesized ancient bodies of water using Mars Orbiter Laser Altimeter (MOLA) data. *Journal of Geophysical Research*, *106*(E2), 3275–3295. https://doi.org/10.1029/2000je001257

Ivanov, M. A., Hiesinger, H., Erkeling, G., Hielscher, F. J., & Reiss, D. (2012). Major episodes of geologic history of Isidis Planitia on Mars. *Icarus*, *218*(1), 24–46. https://doi.org/10.1016/j.icarus.2011.11.029

Ivanov, M. A., Hiesinger, H., Erkeling, G., & Reiss, D. (2014). Mud volcanism and morphology of impact craters in Utopia Planitia on Mars: Evidence for the ancient ocean. *Icarus*, *228*, 121–140. https://doi.org/10.1016/j.icarus.2013.09.018

Jakosky, B. M., & Carr, M. H. (1985). Possible precipitation of ice at low latitudes of Mars during periods of high obliquity. *Nature*, *315*(6020), 559–561. https://doi.org/10.1038/315559a0

Jones, E., Caprarelli, G., & Osinski, G. R. (2016). Insights into complex layered ejecta emplacement and subsurface stratigraphy in Chryse Planitia, Mars, through an analysis of THEMIS brightness temperature data. *Journal of Geophysical Research: Planets*, *121*(6), 986–1015. https://doi.org/10.1002/2015je004879

Kadish, S. J., Barlow, N. G., & Head, J. W. (2009). Latitude dependence of Martian pedestal craters: Evidence for a sublimation-driven formation mechanism. *Journal of Geophysical Research*, *114*(E10), E10001. https://doi.org/10.1029/2008je003318

Kadish, S. J., Head, J. W., Barlow, N. G., & Marchant, D. R. (2008). Martian pedestal craters: Marginal sublimation pits implicate a climate-related formation mechanism. *Geophysical Research Letters*, *35*(16), L16104. https://doi.org/10.1029/2008gl034990

Kirchoff, M. R., & Grimm, R. E. (2018). Timing and distribution of single-layered ejecta craters imply sporadic preservation of tropical subsurface ice on Mars. *Journal of Geophysical Research: Planets*, *123*(1), 131–144. https://doi.org/10.1002/2017je005432

Kneissl, T., van Gasselt, S., & Neukum, G. (2011). Map-projection-independent crater size-frequency determination in GIS environments—New software tool for ArcGIS. *Planetary and Space Science*, *59*(11–12), 1243–1254. https://doi.org/10.1016/j.pss.2010.03.015

Komatsu, G., Ori, G. G., Di Lorenzo, S., Rossi, A. P., & Neukum, G. (2007). Combinations of processes responsible for Martian impact crater "layered ejecta structures" emplacement. *Journal of Geophysical Research*, *112*(E6), E06005. https://doi.org/10.1029/2006je002787

Kreslavsky, M. A., & Head, J. W. (2002). Fate of outflow channel effluents in the northern lowlands of Mars: The Vastitas Borealis formation as a sublimation residue from frozen ponded bodies of water. *Journal of Geophysical Research*, *107*(E12), 5121. https://doi.org/10.1029/2001je001831

Kuzmin, R. O. (1980). Determination of frozen soil depth on Mars from the morphology of fresh craters. In *Akademiia Nauk SSSR, Doklady* (Vol. 252, No. 6, pp. 1445–1448).

Kuzmin, R. O., Bobina, N. N., Zabalueva, E. V., & Shashkina, V. P. (1988). Structural inhomogeneities of the Martian cryolithosphere. *Solar System Research*, *22*(3), 121.

Lagain, A., Servis, K., Benedix, G. K., Norman, C., Anderson, S., & Bland, P. A. (2021). Model age derivation of large martian impact craters, using automatic crater counting methods. *Earth and Space Science*, *8*(2), e2020EA001598. https://doi.org/10.1029/2020EA001598

Li, L., Yue, Z., Di, K., & Peng, M. (2015). Observations of Martian layered ejecta craters and constraints on their formation mechanisms. *Meteoritics & Planetary Sciences*, *50*(3), 508–522. https://doi.org/10.1111/maps.12438

Liu, J., Li, C., Zhang, R., Rao, W., Cui, X., Geng, Y., et al. (2021). Geomorphic contexts and science focus of the Zhurong landing site on Mars. *Nature Astronomy*, *6*, 65–71. https://doi.org/10.1038/s41550-021-01519-5

Lockwood, J. F., Kargel, J. S., & Strom, R. B. (1992). Thumbprint terrain on the northern plains: A glacial hypothesis. In *Lunar and planetary science conference* (Vol. 23).

Lucchitta, B. K. (1982). Ice sculpture in the Martian outflow channels. *Journal of Geophysical Research*, *87*(B12), 9951–9973. https://doi.org/10.1029/jb087ib12p09951

Madeleine, J. B., Forget, F., Head, J. W., Levrard, B., Montmessin, F., & Millour, E. (2009). Amazonian northern mid-latitude glaciation on Mars: A proposed climate scenario. *Icarus*, *203*(2), 390–405. https://doi.org/10.1016/j.icarus.2009.04.037

Madeleine, J. B., Head, J. W., Forget, F., Navarro, T., Millour, E., Spiga, A., et al. (2014). Recent ice ages on Mars: The role of radiatively active clouds and cloud microphysics. *Geophysical Research Letters*, *41*(14), 4873–4879. https://doi.org/10.1002/2014gl059861

Malin, M. C., Bell, J. F., Cantor, B. A., Caplinger, M. A., Calvin, W. M., Clancy, R. T., et al. (2007). Context camera investigation on board the Mars Reconnaissance orbiter. *Journal of Geophysical Research*, *112*(E5). E05S04. https://doi.org/10.1029/2006je002808

Marchenko, A. G., Basilevsky, A. T., Hoffmann, H., Hauber, E., Cook, A. C., & Neukum, G. (1998). Geology of the common mouth of the Ares and Tiu Valles, Mars. *Solar System Research*. Retrieved from http://hdl.handle.net/10088/6380

Masursky, H., Boyce, J. M., Dial, A. L., Schaber, G. G., & Strobell, M. E. (1977). Classification and time of formation of Martian channels based on Viking data. *Journal of Geophysical Research*, *82*(28), 4016–4038. https://doi.org/10.1029/js082i028p04016

McCauley, J. F. (1973). Mariner 9 evidence for wind erosion in the equatorial and mid-latitude regions of Mars. *Journal of Geophysical Research*, *78*(20), 4123–4137. https://doi.org/10.1029/jb078i020p04123

McGill, G. E. (1986). The giant polygons of Utopia, northern Martian plains. *Geophysical Research Letters*, *13*(8), 705–708. https://doi.org/10.1029/gl013i008p00705

McGowan, E. M. (2011). The Utopia/Isidis overlap: Possible conduit for mud volcanism on Mars. *Icarus*, *212*(2), 622–628. https://doi.org/10.1016/j.icarus.2011.01.025

Mellon, M. T., Arvidson, R. E., Sizemore, H. G., Searls, M. L., Blaney, D. L., Cull, S., et al. (2009). Ground ice at the Phoenix landing site: Stability state and origin. *Journal of Geophysical Research*, *114*(E1), E00E07. https://doi.org/10.1029/2009je003417

Mellon, M. T., & Jakosky, B. M. (1995). The distribution and behavior of Martian ground ice during past and present epochs. *Journal of Geophysical Research*, *100*(E6), 11781–11799. https://doi.org/10.1029/95je01027

Mellon, M. T., Jakosky, B. M., & Postawko, S. E. (1997). The persistence of equatorial ground ice on Mars. *Journal of Geophysical Research*, *102*(E8), 19357–19369. https://doi.org/10.1029/97je01346

Melosh, H. J. (1989). *Impact cratering: A geologic process*. icgp.

Meresse, S., Costard, F., Mangold, N., Baratoux, D., & Boyce, J. M. (2006). Martian perched craters and large ejecta volume: Evidence for episodes of deflation in the northern lowlands. *Meteoritics & Planetary Sciences*, *41*(10), 1647–1658. https://doi.org/10.1111/j.1945-5100.2006.tb00442.x

Michael, G. G. (2013). Planetary surface dating from crater size–frequency distribution measurements: Multiple resurfacing episodes and differential isochron fitting. *Icarus*, *226*(1), 885–890. https://doi.org/10.1016/j.icarus.2013.07.004

Michael, G. G., Kneissl, T., & Neesemann, A. (2016). Planetary surface dating from crater size-frequency distribution measurements: Poisson timing analysis. *Icarus*, *277*, 279–285. https://doi.org/10.1016/j.icarus.2016.05.019

Michael, G. G., & Neukum, G. (2010). Planetary surface dating from crater size–frequency distribution measurements: Partial resurfacing events and statistical age uncertainty. *Earth and Planetary Science Letters*, *294*(3–4), 223–229. https://doi.org/10.1016/j.epsl.2009.12.041

Michael, G. G., Platz, T., Kneissl, T., & Schmedemann, N. (2012). Planetary surface dating from crater size–frequency distribution measurements: Spatial randomness and clustering. *Icarus*, *218*(1), 169–177. https://doi.org/10.1016/j.icarus.2011.11.033

Mills, M. M., McEwen, A. S., & Okubo, C. H. (2021). A preliminary regional geomorphologic map in Utopia Planitia of the Tianwen-1 Zhurong landing region. *Geophysical Research Letters*, *48*, e2021GL094629. https://doi.org/10.1029/2021gl094629

Moore, J. M., Clow, G. D., Davis, W. L., Gulick, V. C., Janke, D. R., McKay, C. P., et al. (1995). The circum-Chryse region as a possible example of a hydrologic cycle on Mars: Geologic observations and theoretical evaluation. *Journal of Geophysical Research*, *100*(E3), 5433–5447. https://doi.org/10.1029/94je08205

Mouginis-Mark, P. (1979). Martian fluidized crater morphology: Variations with crater size, latitude, altitude, and target material. *Journal of Geophysical Research*, *84*(B14), 8011–8022.

Mouginis-Mark, P. (1981). Ejecta emplacement and modes of formation of Martian fluidized ejecta craters. *Icarus*, *45*(1), 60–76. https://doi.org/10.1016/0019-1035(81)90006-3

Neukum, G., & Hiller, K. (1981). Martian ages. *Journal of Geophysical Research*, *86*(B4), 3097–3121. https://doi.org/10.1029/jb086ib04p03097

Niu, S., Zhang, F., Di, K., Gou, S., & Yue, Z. (2021). Supporting data for 68 LECs in the two candidate landing areas of China's first Mars mission (Tianwen-1) [Data set]. Zenodo. https://doi.org/10.5281/zenodo.5108950

Noe Dobrea, E. Z., Stoker, C. R., Berman, D. C., McKay, C. P., & Davila, A. F. (2020). Crater morphology and evolution at the Phoenix landing site: Insights into timing of modern geological processes and subsurface ice. *Icarus*, *342*, 113534. https://doi.org/10.1016/j.icarus.2019.113534

Nummedal, D., & Prior, D. B. (1981). Generation of Martian chaos and channels by debris flows. *Icarus*, *45*(1), 77–86. https://doi.org/10.1016/0019-1035(81)90007-5

Oberbeck, V. R. (2009). Layered ejecta craters and the early water/ice aquifer on Mars. *Meteoritics & Planetary Sciences*, *44*(1), 43–54. https://doi.org/10.1111/j.1945-5100.2009.tb00716.x

Parker, T. J., Saunders, R. S., & Schneeberger, D. M. (1989). Transitional morphology in west Deuteronilus Mensae, Mars: Implications for modification of the lowland/upland boundary. *Icarus*, *82*(1), 111–145. https://doi.org/10.1016/0019-1035(89)90027-4

Reiss, D., Hauber, E., Michael, G., Jaumann, R., & Neukum, G. (2005). Small rampart craters in an equatorial region on Mars: Implications for near-surface water or ice. *Geophysical Research Letters*, *32*(10), L10202. https://doi.org/10.1029/2005GL022758

Reiss, D., van Gasselt, S., Hauber, E., Michael, G., Jaumann, R., & Neukum, G. (2006). Ages of rampart craters in equatorial regions on Mars: Implications for the past and present distribution of ground ice. *Meteoritics & Planetary Sciences*, *41*(10), 1437–1452. https://doi.org/10.1111/j.1945-5100.2006.tb00428.x

Robbins, S. J., & Hynek, B. M. (2012). A new global database of Mars impact craters ≥ 1 km: 1. Database creation, properties, and parameters. *Journal of Geophysical Research*, *117*(E5). https://doi.org/10.1029/2011je003966

Robbins, S. J., Runyon, K., Singer, K. N., Bray, V. J., Beyer, R. A., Schenk, P., et al. (2018). Investigation of Charon's craters with abrupt terminus ejecta, comparisons with other icy bodies, and formation implications. *Journal of Geophysical Research: Planets*, *123*(1), 20–36. https://doi.org/10.1002/2017je005287

Salvatore, M. R., & Christensen, P. R. (2014). On the origin of the Vastitas Borealis Formation in Chryse and Acidalia Planitiae, Mars. *Journal of Geophysical Research: Planets*, *119*(12), 2437–2456. https://doi.org/10.1002/2014je004682

Saunders, R. S., Arvidson, R. E., Badhwar, G. D., Boynton, W. V., Christensen, P. R., Cucinotta, F. A., et al. (2004). 2001 Mars Odyssey mission summary. *Space Science Reviews*, *110*(1), 1–36. https://doi.org/10.1007/978-0-306-48600-5_1

Schultz, P. H. (1992). Atmospheric effects on ejecta emplacement. *Journal of Geophysical Research*, *97*(E7), 11623–11662. https://doi.org/10.1029/92je00613

Schultz, P. H., & Gault, D. E. (1979). Atmospheric effects on Martian ejecta emplacement. *Journal of Geophysical Research*, *84*(B13), 7669–7687. https://doi.org/10.1029/jb084ib13p07669

Séjourné, A., Costard, F., Gargani, J., Soare, R. J., Fedorov, A., & Marmo, C. (2011). Scalloped depressions and small-sized polygons in western Utopia Planitia, Mars: A new formation hypothesis. *Planetary and Space Science*, *59*(5–6), 412–422.

Senft, L. E., & Stewart, S. T. (2008). Impact crater formation in icy layered terrains on Mars. *Meteoritics & Planetary Sciences*, *43*(12), 1993–2013. https://doi.org/10.1111/j.1945-5100.2008.tb00657.x

Skinner, J. A., Jr., & Tanaka, K. L. (2007). Evidence for and implications of sedimentary diapirism and mud volcanism in the southern Utopia highland–lowland boundary plain, Mars. *Icarus*, *186*(1), 41–59. https://doi.org/10.1016/j.icarus.2006.08.013

Soare, R. J., Costard, F., Pearce, G. D., & Séjourné, A. (2012). A re-interpretation of the recent stratigraphical history of Utopia Planitia, Mars: Implications for late-Amazonian periglacial and ice-rich terrain. *Planetary and Space Science*, *60*(1), 131–139. https://doi.org/10.1016/j.pss.2011.07.007

Squyres, S. W., Clifford, S. M., Kuzmin, R. O., Zimbelman, J. R., & Costard, F. (1992). Ice in the Martian Megaregolith. *Mars*.

Tanaka, K. L. (1999). Debris-flow origin for the Simud/Tiu deposit on Mars. *Journal of Geophysical Research*, *104*(E4), 8637–8652. https://doi.org/10.1029/98je02552

Tanaka, K. L., Skinner, J. A., Hare, T. M., Joyal, T., & Wenker, A. (2003). Resurfacing history of the northern plains of Mars based on geologic mapping of Mars global surveyor data. *Journal of Geophysical Research*, *108*(E4), 8043. https://doi.org/10.1029/2002je001908

Tanaka, K. L., Skinner, J. A., Jr, Dohm, J. M., Irwin, R. P., III, Kolb, E. J., Fortezzo, C. M., et al. (2014). Geologic map of Mars: U.S. Geological Survey Scientific Investigations Map 3292. scale 1:20,000,000, pamphlet 43 p. https://doi.org/10.3133/sim3292

Viola, D., McEwen, A. S., Dundas, C. M., & Byrne, S. (2015). Expanded secondary craters in the Arcadia Planitia region, Mars: Evidence for tens of Myr-old shallow subsurface ice. *Icarus*, *248*, 190–204. https://doi.org/10.1016/j.icarus.2014.10.032

Wada, K., & Barnouin-Jha, O. S. (2006). The formation of fluidized ejecta on Mars by granular flows. *Meteoritics & Planetary Sciences*, *41*(10), 1551–1569. https://doi.org/10.1111/j.1945-5100.2006.tb00435.x

Wan, W., Wang, C., Li, C., & Wei, Y. (2020). China's first mission to Mars. *Nature Astronomy*, *4*(7), 721. https://doi.org/10.1038/s41550-020-1148-6

Wan, W., Yu, T., Di, K., Wang, J., Liu, Z., Li, L., et al. (2021). Visual localization of the Tianwen-1 lander using orbital, descent and rover images. *Remote Sensing*, *13*(17), 3439. https://doi.org/10.3390/rs13173439

Warner, N., Gupta, S., Muller, J. P., Kim, J. R., & Lin, S. Y. (2009). A refined chronology of catastrophic outflow events in Ares Vallis, Mars. *Earth and Planetary Science Letters*, *288*(1–2), 58–69. https://doi.org/10.1016/j.epsl.2009.09.008

Weiss, D. K. (2019). Mars in ice ages for ∼25% of post-Noachian geologic history. *Earth and Planetary Science Letters*, *528*, 115847.

Weiss, D. K., & Head, J. W. (2013). Formation of double-layered ejecta craters on Mars: A glacial substrate model. *Geophysical Research Letters*, *40*(15), 3819–3824. https://doi.org/10.1002/grl.50778

Weiss, D. K., & Head, J. W. (2014). Ejecta mobility of layered ejecta craters on Mars: Assessing the influence of snow and ice deposits. *Icarus*, *233*, 131–146. https://doi.org/10.1016/j.icarus.2014.01.038

Weiss, D. K., & Head, J. W. (2017). Evidence for stabilization of the ice-cemented cryosphere in earlier Martian history: Implications for the current abundance of groundwater at depth on Mars. *Icarus*, *288*, 120–147. https://doi.org/10.1016/j.icarus.2017.01.018

Weiss, D. K., & Head, J. W. (2018). Testing landslide and atmospheric-effects models for the formation of double-layered ejecta craters on Mars. *Meteoritics & Planetary Sciences*, *53*(4), 741–777. https://doi.org/10.1111/maps.12859

Werner, S. C., & Tanaka, K. L. (2011). Redefinition of the crater-density and absolute-age boundaries for the chronostratigraphic system of Mars. *Icarus*, *215*(2), 603–607. https://doi.org/10.1016/j.icarus.2011.07.024

Wichman, R. W., & Schultz, P. H. (1989). Sequence and mechanisms of deformation around the Hellas and Isidis impact basins on Mars. *Journal of Geophysical Research*, *94*(B12), 17333–17357. https://doi.org/10.1029/jb094ib12p17333

Wohletz, K. H., & Sheridan, M. F. (1983). Martian rampart crater ejecta: Experiments and analysis of melt-water interaction. *Icarus*, *56*(1), 15–37. https://doi.org/10.1016/0019-1035(83)90125-2

Woronow, A. (1981). Preflow stresses in martian rampart ejecta blankets: A means of estimating the water content. *Icarus*, *45*(2), 320–330. https://doi.org/10.1016/0019-1035(81)90037-3

Wu, B., Dong, J., Wang, Y., Li, Z., Chen, Z., Liu, W. C., et al. (2021). Characterization of the candidate landing region for Tianwen-1–China's First mission to Mars. *Earth and Space Science*, *8*, e2021EA001670. https://doi.org/10.1029/2021EA001670

Wu, X., Liu, Y., Zhang, C., Wu, Y., Zhang, F., Du, J., et al. (2021). Geological characteristics of China's Tianwen-1 landing site at Utopia Planitia, Mars. *Icarus*, *370*, 114657. https://doi.org/10.1016/j.icarus.2021.114657

Wulf, G., & Kenkmann, T. (2015). High-resolution studies of double-layered ejecta craters: Morphology, inherent structure, and a phenomenological formation model. *Meteoritics & Planetary Sciences*, *50*(2), 173–203. https://doi.org/10.1111/maps.12416

Xiao, Z., & Komatsu, G. (2013). Impact craters with ejecta flows and central pits on Mercury. *Planetary and Space Science*, *82*, 62–78. https://doi.org/10.1016/j.pss.2013.03.015

Ye, P., Sun, Z., Rao, W., & Meng, L. (2017). Mission overview and key technologies of the first Mars probe of China. *Science China Technological Sciences*, *60*(5), 649–657. https://doi.org/10.1007/s11431-016-9035-5

Zhao, J., Xiao, Z., Huang, J., Head, J. W., Wang, J., Shi, Y., et al. (2021). Geological characteristics and targets of high scientific interest in the Zhurong landing region on Mars. *Geophysical Research Letters*, *48*(20), e2021GL094903. https://doi.org/10.1029/2021GL094903

Zhou, B., Shen, S., Lu, W., Liu, Q., Tang, C., Li, S., et al. (2020). The Mars rover subsurface penetrating radar onboard China's Mars 2020 mission. *Earth and Planetary Physics*, *4*(4), 345–354. https://doi.org/10.26464/epp2020054

Zou, Y., Zhu, Y., Bai, Y., Wang, L., Jia, Y., Shen, W., et al. (2021). Scientific objectives and payloads of Tianwen-1, China's first Mars exploration mission. *Advances in Space Research*, *67*(2), 812–823. https://doi.org/10.1016/j.asr.2020.11.005